Advanced Drug Delivery Reviews 138 (2019) 133–147

Contents lists available at ScienceDirect

Advanced Drug Delivery Reviews

journal homepage: www.elsevier.com/locate/addr

Review article

Light-responsive nanomedicine for biophotonic imaging and targeted therapy

Jihwan Son [a,b,1], Gawon Yi [a,b,1], Jihye Yoo [a,b], Changhee Park [a,b], Heebeom Koo [a,b,c,*], Hak Soo Choi [d,**]

[a] Department of Medical Lifescience, The Catholic University of Korea, 222 Banpo-daero, Seocho-gu, Seoul, 06591, Republic of Korea
[b] Department of Biomedicine & Health Sciences, The Catholic University of Korea, 222 Banpo-daero, Seocho-gu, Seoul, 06591, Republic of Korea
[c] Catholic Photomedicine Research Institute, College of Medicine, The Catholic University of Korea, 222 Banpo-daero, Seocho-gu, Seoul, 06591, Republic of Korea
[d] Gordon Center for Medical Imaging, Department of Radiology, Massachusetts General Hospital, Harvard Medical School, Boston, MA 02114, USA

ARTICLE INFO

Article history:
Received 1 May 2018
Received in revised form 16 August 2018
Accepted 8 October 2018
Available online 12 October 2018

Keywords:
Light-responsiveness
Nanomedicine
Optical imaging
Targeted therapy

ABSTRACT

Nanoparticles (NPs) play a key role in nanomedicine in multimodal imaging, drug delivery and targeted therapy of human diseases. Consequently, due to the attractive properties of NPs including high stability, high payload, multifunctionality, design flexibility, and efficient delivery to target tissues, nanomedicine employs various types of NPs to enhance targeting and treatment efficacy. In this review, we primarily focus on light-responsive materials, such as fluorophores, photosensitizers, semiconducting polymers, carbon structures, gold particles, quantum dots, and upconversion crystals, for their biomedical applications. Armed with these nanomaterials, NPs represent a growing potential in biophotonic imaging (luminescence, photoacoustic, surface enhanced Raman scattering, and optical coherence tomography) as well as targeted therapy (photodynamic therapy, photothermal therapy, and light-responsive drug release).

Contents

* Corresponding author at: Department of Medical Lifescience, College of Medicine, The Catholic University of Korea, 222 Banpo-daero, Seoul 06591, Republic of Korea.
** Corresponding author at: Gordon Center for Medical Imaging, Department of Radiology, Massachusetts General Hospital and Harvard Medical School, Boston, MA 02114, USA
E-mail addresses: hbkoo@catholic.ac.kr (H. Koo), hchoi12@mgh.harvard.edu (H.S. Choi).
[1] These authors contributed equally.

https://doi.org/10.1016/j.addr.2018.10.002
0169-409X/

1. Introduction

Fiat Lux: From the beginning of mankind, light has been one of the most important stimuli to living organisms. The characteristics and functions of light vary dependent upon its wavelength and, thus, its biological and biomedical applications can also be diverse [1–3]. Among the broad spectrum of light, wavelengths from about 400 to 800 nm are relatively familiar and widely used without special devices (Fig. 1). Ultraviolet (UV) light (200–400 nm) is invisible to most humans and has generally been used for disinfection [4]. Some chemicals with benzene rings are UV absorbent and can be detected using handy UV lamps for synthesis and purification [5,6]. UV light is also frequently used to trigger polymerization with photo-initiators. In particular, azobenzenes undergo *trans*-to-*cis* photo-isomerization upon UV light irradiation, so that azobenzene functionalized materials can change their structure in response to UV [5]. 2-Nitrobenzyl linkers are also frequently used for UV cleavage of photodegradable hydrogels [6]. However, UV light may damage biological components, which limits its biomedical application as an external trigger. Visible light (400–650 nm) is more generally utilized for various fluorophores and proteins due to the advantage of being observable with the naked eye. Consequently, visible light-sensitive nanomaterials have been extensively developed for *in vitro* diagnosis; however, their utility in *in vivo* imaging has been limited due to superficial tissue penetration [3]. In addition, many endogenous fluorophores in the body, including epidermis pigments, hemoglobins, and chlorophylls, absorb light energy in the range of 200–650 nm which causes autofluorescence during optical imaging (Fig. 1). Nonetheless, near-infrared (NIR; 650–900 nm) fluorescence is advantageous for biophotonic imaging because of the low absorption of hemoglobin and water as well as minimal to low autofluorescence, resulting in deep tissue penetration of NIR light [1]. Many chemists, biologists, and materials scientists have therefore intensively studied NIR fluorophores by formulating with small molecules, peptides, proteins, and NPs for their clinical and biomedical applications [1–3,7]. (See Table 1.)

In particularly, nanomedicine utilizes clinical NPs that are highly soluble in aqueous solution, highly stable in serum and biological environments, and are easy to use in terms of formulations, multifunctionality, and high payload of small molecules, peptides, proteins, and antibodies [8,9]. For example, Doxil and Abraxane are the representative NPs that are FDA-approved formulations to carry doxorubicin and paclitaxel, respectively, for efficient chemotherapy [10]. Since the physicochemical and biological properties of NPs are the main drivers of the clinical success of nanomedicine in bioimaging, drug delivery, and therapeutic applications, "smart" NPs that change their structure and functionality in response to specific internal and external stimuli have been extensively developed [11–13]. Among them, as explained above, light has been extensively utilized as an external stimulus because it is non-contact, clean, and can be turned on and off rapidly [14]. Consequently, biophotonics has led the field of photonics and optical techniques towards biomedical applications by using a wide range of light from UV–visible to NIR for imaging, diagnosis, surgery, and therapy of human diseases. In this review, we discuss recent advances in light-responsive NPs and their biophotonic imaging uses, including in luminescence, photoacoustic (PA), surface enhanced Raman scattering (SERS), and optical coherence tomography (OCT). Furthermore, we introduce recent developments in therapeutic nanomedicine for photodynamic therapy (PDT), photothermal therapy (PTT), and light-responsive drug release (Table 1).

2. Light-responsive nanomaterials

For biological or biomedical applications, various types of nanomaterials have been developed using light-responsive components mainly composed of organic materials (fluorophores, photosensitizers, and carbon-based NPs) and inorganic-based NPs (gold NPs, quantum dots, and upconverting NPs) [8]. The intrinsic characteristics of these components greatly influence optical functions and physicochemical properties of the final form of nanomaterials. Since there are a wide range of NPs and fluorophores available for engineering unique light-responsive nanomaterials, the field of biophotonic imaging and targeted therapy has advanced extensively in recent years. These NPs are mostly multifunctional, therefore, one can be used for both imaging and theranostics, which has stimulated the fields of molecular imaging, tissue engineering, cancer diagnostics, drug delivery, and many other biomedical applications.

2.1. Organic nanomaterials

Fluorophores are representative light-responsive materials, which absorb light energy and emit photons with particular wavelengths [3,39]. By simple loading or conjugating dyes to the targeting domain, such as small molecule ligands, peptides, proteins, antibodies, and polymers, many imaging nanoprobes have been developed and applied in bioimaging and therapy [7,9,40–46]. Atreya et al. conjugated fluorescein isothiocyanate (FITC) on an adalimumab antibody for *in vivo* imaging of membrane-bound tumor necrosis factor (mTNF) [47]. FITC-

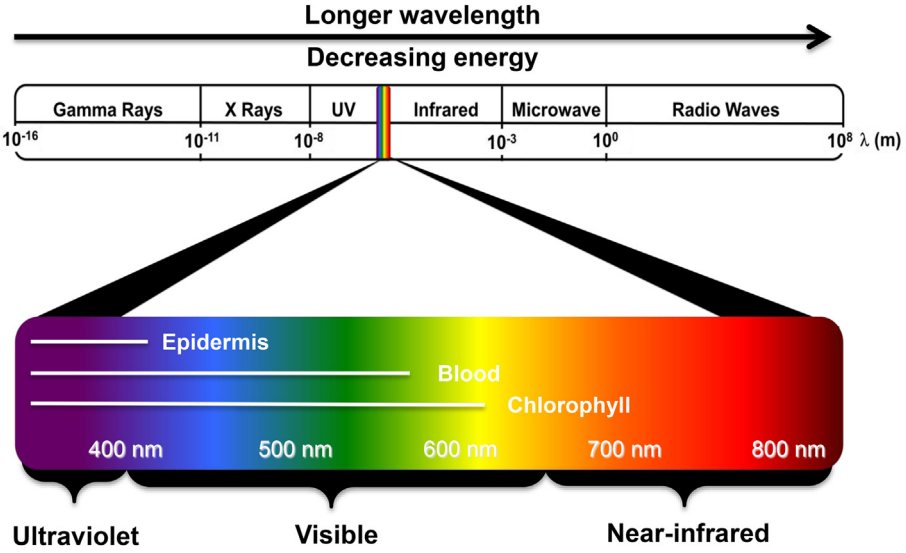

Fig. 1. Wavelength ranges of the electromagnetic radiation spectrum. The light spectral range extends from gamma rays to radio waves and visible radiation includes 400–800 nm that can be observed by the human eye [3].

Table 1
Summary of recently developed light-responsive nanomedicines.

Application		λ_{ex} (nm)	Type of NPs	Ref.
Photonic imaging	Luminescence	532	Photon upconversion NPs	[15,16]
		550	ZGGO:Cr NPs	[17]
		796	Cyclodextrin-based NPs	[18]
	PA	750	Graphene-coated gold nanorods	[19]
		700	Semiconducting phthalocyanine NPs	[20]
		675	Semiconducting perylene diimide NPs	[21]
	SERS	785	Silica-coated gold nanostars	[22,23]
	OCT	800	Gold nanorods	[24,25]
Targeted therapy	PDT	none	Photosensitizer-conjugated luciferase	[26]
		800	Aggregation-induced emission carbon dots	[27]
		635	Magnetofluorescent carbon dots	[28]
		650	Cu-containing metal-organic NPs	[29]
	PTT	808	Polydopamine-coated spiked gold NPs	[30]
		1064	Polypyrrole nanosheet	[31]
		980	Copper sulfide NPs	[32]
		808	Glucose oxidase-Prussian blue NPs	[33]
	Drug delivery	730	Lipid biallylic hydrogen liposome	[34]
		808	Gold nanorod-lipid bilayer liposome	[35]
		808	Renal clearable ultrasmall gold NPs	[36]
		690	Photosensitizer-lipid bilayer liposome	[37]
		638	Photosensitizer-red blood cell NPs	[38]

adalimumab was topically administered to 25 patients with Crohn's disease, the intestinal immune cells expressing mTNF were observed by confocal laser endomicroscopy based on fluorescence imaging. In particular, the fluorescence emission of neighboring dyes can be turned off while they get close to the quenching molecules and turned on after cleavage or release [48]. Lee et al. linked NIR fluorescent Cy5.5 to black-hole-quencher 3 cleavable by a matrix metalloproteinase (MMP) that is abundant in tumor tissue. This Cy5.5-MMP peptide conjugate was then attached to the surface of glycol chitosan NPs, and was shown to massively target tumoral tissue in SCC7 tumor-bearing mice and an azoxymethane-treated colon cancer model [48].

Many fluorophores can also be used as photosensitizers (PSs) that generate toxic reactive oxygen species (ROS) along with fluorescence upon light irradiation [49–51]. Porphyrin-based PSs such as hematoporphyrin or protoporphyrin IX were the first-generation of PSs and have been treated for more than a million patients in clinical trials [52]. In late 1980s, the second-generation of PSs were developed based on chlorins, pheophorbides, or phtalocyanines, which have longer wavelengths in the NIR window providing deeper tissue penetration and better therapeutic efficacy [49–51]. Since most PSs are hydrophobic, highly water-soluble NP formulations are required. Roy et al. entrapped a water-insoluble PS, 2-devinyl-2-(1-hexyloxyethyl) pyropheophorbide, into silica NPs, which were stably dispersed in water [49]. Upon 650 nm laser irradiation, the silica NPs containing PSs killed Hela and UCI-107 tumor cells effectively. Target-specific delivery of PSs also can be achieved by conjugating a phthalocyanine PS (*e.g.*, IR700) to panitumumab to targeting human epidermal growth factor receptor 1 (HER1) [50]. IR700-HER1 antibody conjugates showed successful tumor growth suppression by PDT in HER1-positive A431 tumor models. In clinical applications, Visudyne is a representative NP formulation containing PSs that are currently used for PDT [53]. Visudyne is mainly composed of verteporfin in a liposomal structure that has been used for the treatment of age-related macular degeneration [53].

On the other hand, polymers containing multiple aromatic rings, such as polypyrrole (PPy) and polyaniline, generally have strong light absorption and are useful for PTT [51]. As shown in Fig. 2, during the doping process of polyaniline, the transition from emeralidine base to emeralidine salt resulted in a red-shift of its absorption wavelength to the NIR region. They encapsulated polyaniline with amphiphilic polyethylene glycol (PEG)-stearate resulting in stable NPs. Hydrophilic PEG coating has been used as a balancing domain on the surface of NPs to improve stability during systemic circulation and prevent opsonization by the liver by compensating the charge, hydrophobicity, and other physicochemical properties of NPs [8,9]. Generally, PEGylation increases blood half-life of NPs and promotes the enhanced permeation and retention (EPR) effect for improved delivery to the target (see below). Upon NIR laser irradiation at 808 nm, these NPs showed a photothermal effect in killing the adjacent tumor cells in A431 tumor-bearing mice [51].

Carbon-based NPs, such as carbon nanotube and graphene, are also attractive nanomaterials for bioimaging and nanomedicine because of their NIR light absorption and photothermal effect. Carbon nanotubes have a hollow rolled structure of sp^2-hybridized carbon atoms, and graphene is composed of a one-atom-thick single layer of the same benzene rings [8]. For example, Yang et al. modified a nanographene sheet with PEG and labeled with NIR emitting Cy7 [54]. Large sized NPs, typically ranging from 10 to 500 nm, but not limited to 10 nm, generally penetrate through fenestrate vessel walls in angiogenic tissues such as tumors or arthritis and accumulate in the tumoral site by the EPR effect [55]. These carbon-based NPs also showed enhanced blood circulation and high uptake in the 4 T1 tumor, which when followed by PTT using 808 nm laser irradiation resulted in complete destruction of tumors [54]. A drawback of carbon-based NPs, however, is their biocompatibility that has not been fully evaluated yet. These NPs are mainly composed of non-degradable covalent bonds, of which toxicity has been reported *in vitro* and *in vivo* that need to be overcome for human applications [56].

2.2. Inorganic nanomaterials

Gold NPs have special surface plasmon resonance-enhanced light absorbance and scattering properties, which have been used for fluorescence enhancing/quenching, SERS, PA imaging, and PTT [36,57–59]. Notably, the wavelength of light absorbance can be changed by the shape of gold NPs, and NIR absorbing nanorods and nanocages have been preferred for *in vivo* applications. For example, Huang et al. proved that the absorption wavelength of gold nanorods could be tuned by varying their aspect ratio [59]. Nanorods with an aspect ratio of 3.9 could absorb light at 800 nm, and were further conjugated with anti-epidermal growth factor receptor (anti-EGFR) monoclonal antibodies. After incubation with cells, light scattering images could be obtained based on the scattering of nanorods from orange to red light due to the longitudinal surface plasmon oscillation. Exposure of anti-EGFR/Au nanorods to the red laser of 10 W/cm^2 caused injury and death in malignant cells because the absorbed NIR light was converted into heat at the cell membrane [59].

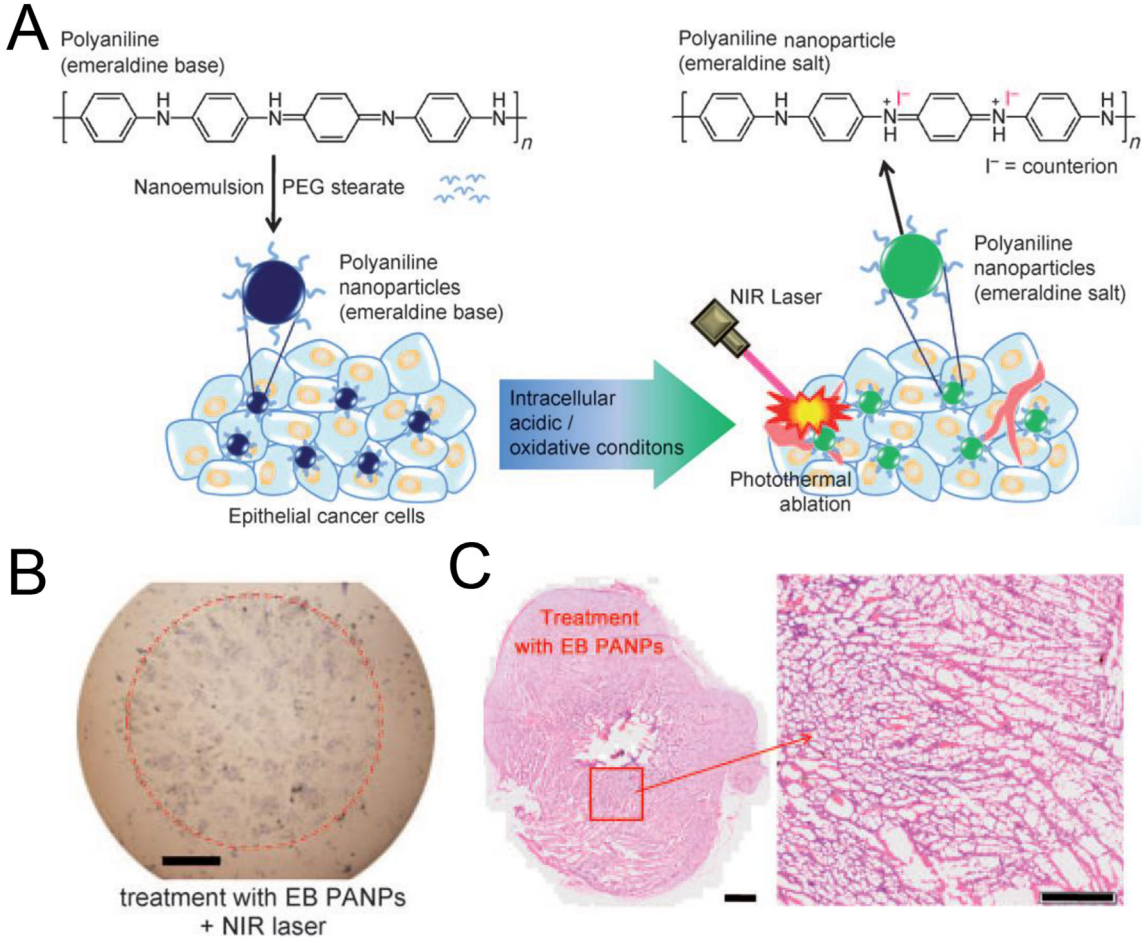

Fig. 2. Light-responsive organic semiconducting polymer NPs: (A) Chemical structure and mechanism of polyaniline-based NPs for photothermal therapy. Images of (B) cells and (C) tissues after treatment and laser irradiation. Reproduced with permission from [51].

Quantum dots (QDs) are nanometer-scaled small semiconductor particles composed of a heavy metal core-shell and an organic coating. QDs absorb a broad range of light and emit red-shifted light up to the NIR window depending on the size of the core [60–64]. QDs generally have high optical properties (*i.e.*, high extinction coefficient, quantum yield) and photostability with negligible photobleaching, and have shown great utility in *in vitro* analysis. However, QDs are mainly composed of heavy metals that are potentially toxic, resulting in limited clinical applications [8,65]. Choi et al. explored the effects of varying the surface coating and hydrodynamic diameter (HD) on biodistribution and clearance of QDs, and achieved selective targeting without any specific targeted moieties [60]. As shown in Fig. 3, intraoperative fluorescence imaging shows that PEG2-coated QDs accumulated in the liver as a result of the reticuloendothelial system because their ultra-short chains on the surface coating retain a hydrophobic character. Interestingly, PEG4-QDs can be readily excreted by renal clearance to the urinary bladder. However, the size of PEG8-QDs is above threshold for renal clearance and thus they accumulated in pancreas, while PEG14-QDs show hepatobiliary clearance through the liver to the intestine with no signal in the kidney. After intravenous injection, the biggest PEG22-QDs remained in the vasculature for over 4 h and accumulated in lymph nodes [60]. These results demonstrated the importance of the physicochemical characteristics of NPs in determining their biodistribution and secretion as well as the usefulness of QDs in *in vivo* imaging [8].

Photon upconversion is the absorption of two or more photons leading to the emission of light at a shorter wavelength than the excitation wavelength [15,16]. The energy conversion process of upconverting nanoparticles (UCNPs) can enhance the depth of penetration and reduce autofluorescence in the body by excitation of long wavelengths. Park et al. incorporated Ce6 PS in UCNPs, which emitted short wavelength light and excited Ce6 in UCNPs to generate ROS for PDT [16]. These UCNPs have two emission lights which are green emission for imaging and red for excitation of Ce6. An *in vivo* study using U87MG tumor-bearing mice showed that the UCNPs accumulated and remained in tumor tissue, which generated signals for both optical and magnetic resonance imaging for 24 h post-injection. When U87MG tumors were irradiated using a 980 nm laser for 5 min, the UCNPs induced complete suppression of tumor growth in the same group of mice [16].

Besides organic NPs that are mostly fabricated by self-assembly of lipids or polymers, inorganic NPs are generally synthesized by growing crystals from metal atoms [66,67]. Thus, metal-based inorganic NPs dissociate slowly or avoid dissociation after cellular uptake compared with liposomes or polymeric micelles. Consequently, their long-term fate and toxicity after diagnostic or therapeutic actions needs to be investigated more carefully. Generally, gold is considered nontoxic; however, some changes in genetic functions were reported after exposure to gold NPs, which may not meet the safety standards for FDA approval [68]. In addition, the amount of salts accompanying gold NPs may cause other toxicity [69]. The potential toxicity of QDs is well-known because they are composed of toxic heavy metals such as cadmium, selenium, tellurium, arsenic, or lead [62,63], which is intensively discussed in Ref. [8]. Regarding UCNPs, there are only a few reports in literature discussing their potential toxicities [70,71]; however, this does not mean that they are biocompatible for clinical use.

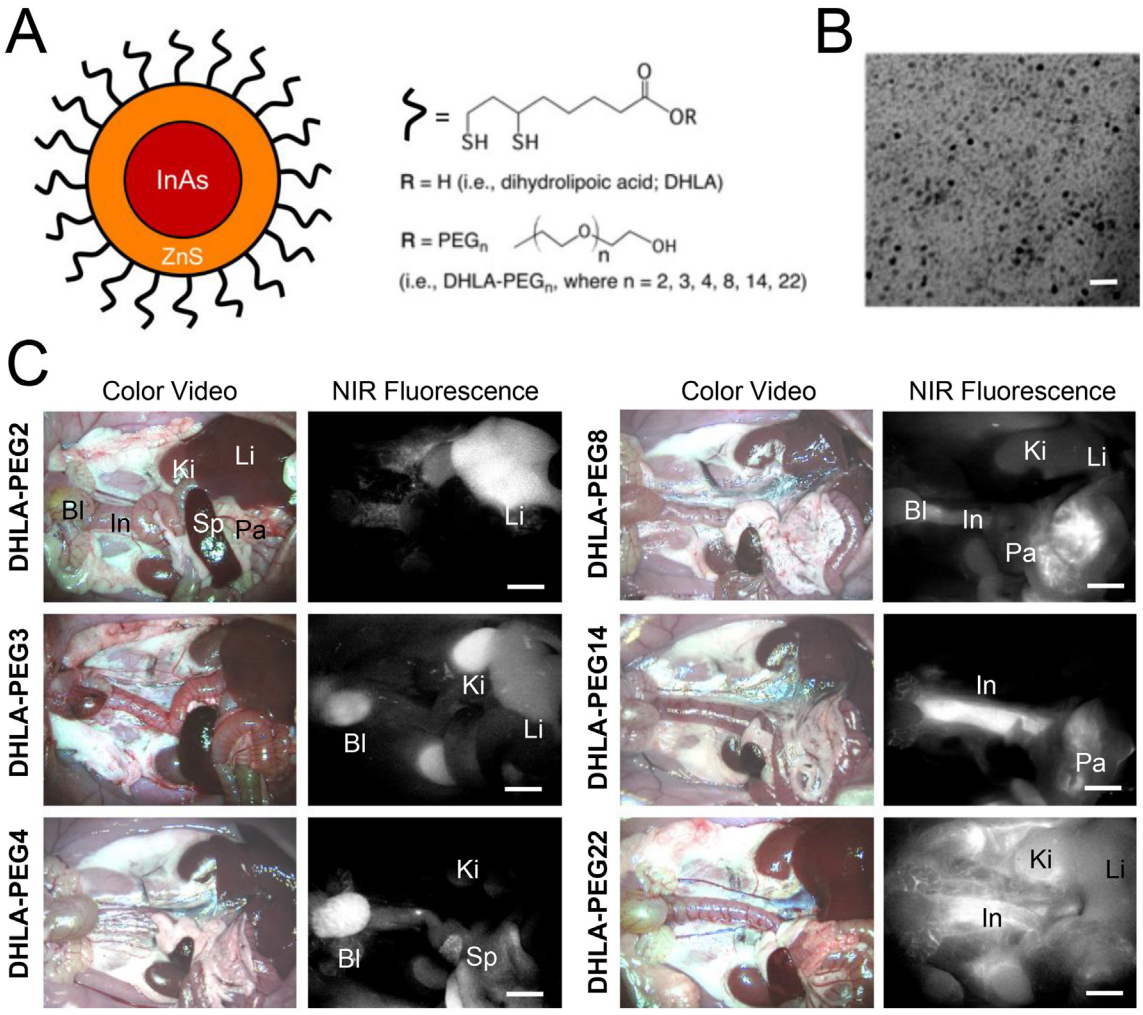

Fig. 3. Inorganic quantum dots (QDs) with high quantum yield and without photo bleaching: (A) InAs(ZnS) QDs with systematically increasing PEG chain length attached through a DHLA linker. (B) TEM of InAs(ZnS)-DHLA-PEG4 (core + shell = 3.2 nm). Scale bar = 10 nm. (C) *In vivo* NIR fluorescence imaging of NIR QDs in Sprague-Dawley rats 4 h post-injection. Abbreviations used are: Ki, kidneys; Bl, bladder; Li, liver; Pa, pancreas; Sp, spleen; and In, intestine. Scale bar = 500 μm. Reproduced with permission from [60].

3. Light-responsive nanomedicine for biophotonic imaging

Seeing (imaging) is the initial step of curing disease. From traditional luminescence imaging to relatively new imaging techniques including NIR, PA, and SERS, researchers have used light to diagnosis various human diseases with the assistance of light-responsive nanomaterials. Armed with the development in biophotonic imaging that combines light-based photonics and optical imaging technology to investigate detailed biological and physiological phenomena in the living organisms, smart nanomedicine has grown by leaps and bounds over the last decade.

3.1. Luminescence imaging

Luminescence is light emission by certain materials with chemical or physical processes, which differs from incandescence based on heating. It includes photoluminescence such as fluorescence or phosphorescence, chemiluminescence, and electroluminescence. Among them, fluorescence imaging is the most representative biophotonic that utilizes light broadly from microscopic imaging to intraoperative NIR image-guided surgery [3,72]. Since autofluorescence and superficial tissue penetration depth are the two main challenges of *in vivo* fluorescence imaging, many efforts have been focused on developing special methodologies to overcome these limitations. Autofluorescence is the emitted light from the background tissues due to the endogenous biomolecules, which increases with the intensity of the excitation light. Because most imaging signals are analyzed based on signal-to-background ratio (SBR), reducing autofluorescence as well as enhancing the brightness of fluorophore itself are highly important [41]. As introduced, NIR window (650–900 nm) is advantageous because of the low tissue attenuation resulting in minimum background autofluorescence [3,9]. Classically, fluorophores are at the ground state energy level (S_0) in a singlet state, and move to excited state (S_n) by light absorption as depicted in the Jablonski diagram [9]. Then, they return to the ground state again by generating fluorescence, so that control of the energy and retention at the excite state is highly important for imaging. Besides this traditional mechanism, Park et al. focused on the triplet-triplet annihilation upconversion (TTA-UC) effect based on a pair of dyes, sensitizer and annihilator [15]. In this system, when one sensitizer in a singlet state is excited to a triplet state by light irradiation, it generates triplet-triplet annihilation between two excited triplet annihilators through triplet-triplet energy. The upconversion light then emits higher energy than the input, thus this ultralow-power imaging could reduce autofluorescence from normal tissue due to low photon energy. Park et al. developed a rationally-designed metal-organic NP with a TTA-UC dyad and observed fluorescence signals at sentinel lymph nodes upon laser irradiation with an ultralow-power density of 5 mW/cm^2 [15].

Luminescence light without excitation can avoid autofluorescence from surrounding background tissues. Wang et al. tried to overcome autofluorescence interference by using persistent luminescence [17].

Interestingly, the selected ZGGO:CR NPs showed intense luminescence without background autofluorescence even 10 h post-irradiation. For comparison, cyanine dye ($\lambda_{em} = 670$ nm) and Ag_2Se ($\lambda_{em} = 740$ nm) were also injected subcutaneously, and their autofluorescence was compared using IVIS Lumina. The mice injected with ZGGO:CR NPs displayed persistent luminescence after cessation of light, while the other mice injected with exogenous fluorochrome showed strong background signals due to the excitation light.

Limited tissue penetration depth is another fundamental challenge of reflectance-based fluorescence imaging [3,9]. Albeit deeper tissue penetration of NIR-Ia light (650–900 nm) compared to visible light (400–650 nm), the maximum tissue imaging depth is limited to 5 mm [9]. However, fluorophores in the NIR-Ib (900–1000 nm) and the NIR-II window (1000–1700 nm) opened a new opportunity for deep tissue imaging over 5 mm under InGaAs sensor-incorporated cameras [73,74]. Despite high water absorption, most endogenous biomolecules (*e.g.*, lipids, hemoglobins, and proteins) have low tissue absorption and extremely low scattering by tissue components in the NIR-II window. In addition, many efforts have been focused on developing NIR-II fluorophores, such as rare-earth-doped NPs, carbon dots, carbon-based NPs including single-walled carbon nanotubes, and organic dyes for superficial vascular imaging, tumor imaging, lymphangiography, and lymph node identification [73–75]. However, further exploration of the translation of these fluorophores to the clinic is necessary, particularly focused on their poor stability in biological media (*i.e.*, hydrophobicity), limited functionality, and potential immunogenicity and toxicity [73].

Another strategy to increase SBR is minimizing the nonspecific accumulation of contrast agents in normal tissue by modulating their surface properties and optimizing their biodistribution and clearance. In 2016, Kang et al. suggested that H-Dots would be ideal to target specific disease sites as unbound particles would be rapidly eliminated from background tissues to the bladder [18]. As shown in Fig. 4, H-Dots are composed of β-cyclodextrins (β-CDs)-conjugated on ε-polylysine (CDPL) for efficient drug delivery and an NIR fluorophore ZW800 for bioimaging [76]. The primary amines of EPL were conjugated with aldehyde-CDs resulting CDPLs, and ZW800-1C was fused to the terminal amine of the polymer. Then, controlled conjugation of the remaining amines with succinic anhydride or acetic anhydride resulted in CDPLs with positive, zwitterionic, negative, or non-charges. Their size was purposely designed to be smaller than 5.5 nm to promote rapid renal clearance from the kidneys to the bladder [36,62,77,78]. This represents a totally different approach to the traditional targeting strategy of NPs over 100 nm which was based on long blood circulation and the EPR effect for passive targeting [8,9]. When injected intravenously into tumor-bearing mice, ZW800-CDPLs circulate systemically in the major organs during blood distribution, target tumor site *via* active targeting, and, more importantly, unbound molecules are eliminated to the bladder within 4 h post-injection. Among various surface charges, zwitterionic ZW800-CDPLs achieved the fastest plasma clearance and highest volume of distribution values. This property is specially advantageous for bioimaging and nanomedicine due to the increase in SBR and decrease in potential toxicity, which together can accelerate the FDA approval of NPs for human usage [18,79].

3.2. Photoacoustic (PA) imaging

PA imaging uses non-ionizing laser pulses to the target molecules or tissues and detects the structural changes by ultrasound imaging [19]. The delivered energy is absorbed and partially transformed into heat, resulting in thermoelastic expansion and ultrasonic emission. The advantages of PA imaging are non-ionization, non-invasiveness, and extremely high resolution, which together enable real-time intraoperative imaging. Basically, PA imaging can be performed without a contrast agent because endogenous molecules, such as water, lipid, hemoglobin, and melanin, can absorb electromagnetic energy and generate acoustic waves [80], but the use of exogenous imaging probes increases PA signals on the target tissue. Therefore, many types of fluorophores, polymer conjugates, carbon NPs, and gold NPs have been used as photoacoustic contrast agents [81]. For *in vivo* imaging, small molecule fluorophores can provide good tissue penetration and low toxicity, while low photostability is their limitation. On the other hand, metal-based, carbon-based, and polymer-based NPs can improve optical properties including photostability, while potential toxicity is the major concern for their clinical use. Liu et al. proved that an orderly arrangement of small gold NPs on larger vesicles can generate an enhanced PA effect [82]. They synthesized 13 nm block copolymer-modified gold NPs and assembled them precisely to generate hollow vesicles with strings of gold NPs on the surface, thereby generating strong coupling, which resulted in enhanced NIR absorption. After subcutaneous injection into the flanks of mice and irradiation using a pulsed laser at 780 nm, these chain vesicles enhanced the PA signal about 8-fold compared to the control non-chain vesicles [82].

To enhance the PA effect, Moon et al. used graphene oxide coating on gold nanorods [19]. As shown in Fig. 5, gold nanorods were synthesized using cetyltrimethylammonium bromide, of which cationic charges attracted the anionic charged nanographene oxides on the surface. Then, the graphene oxide underwent reduction by hydrazine or a xenon lamp that generated an approximately 2.5 nm graphene layer with strong absorption at 750 nm. Furthermore, this gold nanorod showed superior photothermal stability after irradiation with a high-power laser (20 mJ/cm^2) for 5 min while the plasmonic bands of control nanorods at 750 nm were collapsed. Along with gold NPs, semiconducting polymers with strong light absorption can also be used as PA imaging probes [20]. Xie et al. designed *ca.* 20 nm sized gold NPs by conjugating phthalocyanine and PEG, where the PA signal could be amplified according to the size of the semiconducting NPs. In response to ROS, the hydrophilic PEG chains detached while the hydrophobic phthalocyanine cores remained and were able to self-assemble by hydrophobic interactions and π-π stacking into larger NPs up to 500 nm. During this process, the PA signal increased from 1.0 to 1.4 according to the regrowth of the NPs due to increased heat transfer. The NPs showed efficient accumulation into tumoral tissue by the EPR effect and provided an intense PA signal with increased ROS concentration in 4 T1 tumor-bearing mice [20].

As previously reported [55,83], changes in the size of NPs have a significant impact on biodistribution and targeting *in vivo* as well as on PA signals. Yang et al. precisely controlled the size of perylene diimide-based semiconducting NPs by tuning the concentration of diimide molecules during self-assembly [21]. As the size increased from 30 nm to 200 nm, the PA intensity of the NPs increased proportionally. These NPs were used along with PA imaging in lymph node mapping for cancer diagnosis and, interestingly, the 60 nm NPs showed the best targeting in U87MG tumor-bearing mice demonstrating the importance of NP size for *in vivo* application [21].

3.3. Surface-enhanced Raman scattering (SERS)

SERS imaging is an optical imaging technique using inelastic photon scattering during interactions with matter [22,23]. Raman dyes can generate unique Raman spectra-like fingerprints and the signals get stronger when dyes get close to a metal surface. SERS imaging is free from the limitations of traditional fluorescence imaging, including photobleaching of dyes and false positive signals from the naturally emitted light from tissues, although increasing outcome signal strength is still a challenge. Recently, the Kircher group introduced a new concept for surface-enhanced resonance Raman scattering (SERRS) with orders-of-magnitude-higher signals [22]. The very close contact of SERS dyes to the metal surface makes resonance with the incident detection laser. Based on this, they fabricated gold nanostars with red-shifted surface plasma resonance in the NIR region and ionic NIR SERS dyes. These SERRS nanostars generated about a 400-fold enhancement of the Raman signals relative to traditional SERS imaging NP probes, which enabled successful tumor imaging using SERS in mouse models

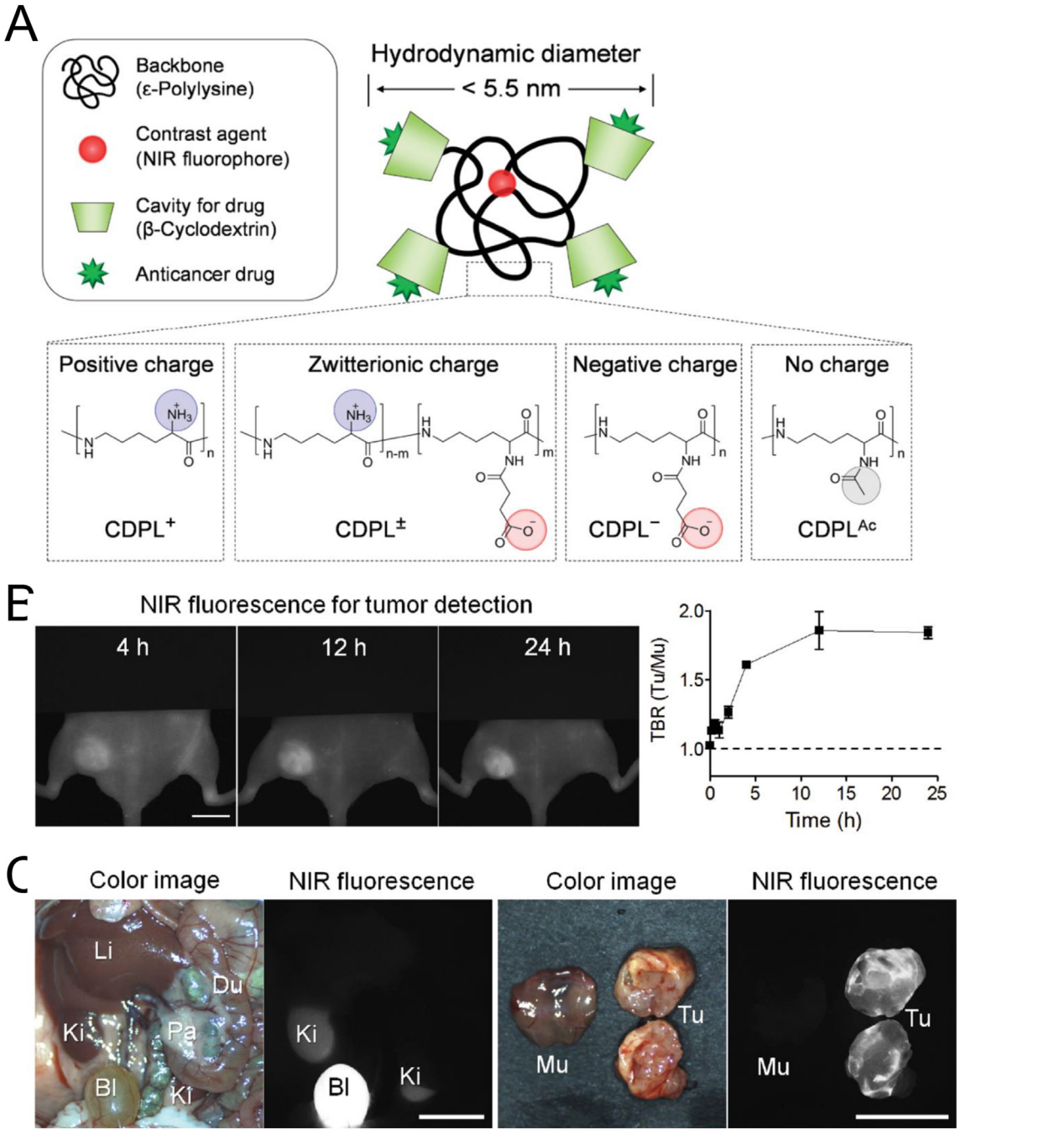

Fig. 4. NIR fluorescence imaging with light-responsive NPs: Polymeric NPs show fast renal clearance but a high signal to background ratio (SBR) in the tumor. (A) Polymer-based nanocarriers and charge variations. (B) Tumor targeting and drug delivery of a zwitterionic inclusion complex with imatinib in xenograft GIST-bearing mice. (C) Biodistribution and tumor targeting 24 h after intravenous injection. Abbreviations used are: Du, duodenum; Mu, muscle; Li, liver; Ki, kidney; Pa, pancreas Tu, tumor. Scale bars, 1 cm. Reproduced with permission from [18].

of pancreatic ductal adenocarcinoma, breast cancer, fibrosarcoma, and prostate cancer. In the subsequent paper, they further increased the specificity of SERS imaging using a ratiometric method with two gold nanostars with or without decoration of the folates [23]. It is hypothesized that folate-modified NPs have a similar biodistribution with unmodified NPs but exhibit enhanced binding to tumors. As shown in Fig. 6, luciferase-transduced SKOV-3 ovarian cancer cells were injected intraperitoneally into mice and tumor growth was imaged using bioluminescence. Then, the two gold nanostars were applied topically and analyzed by SERS imaging, which enabled successfully detection of tiny tumors smaller than 0.5 mm [23].

*3.4. Optical coherence tomography **(OCT)***

OCT provides noninvasive tomographic imaging of internal tissues with high resolution 2D or 3D cross-sectional images [84]. In particular, OCT has been highly useful in ophthalmology to analyze optic nerves and the retinal nerve layer and in measuring the stiffness of the cornea [85]. Light-responsive NPs are useful in OCT imaging and enable further applications based on the measurement of back-reflected or backscattered light [24,25]. For example, the Oldenburg group reported that gold nanorods could provide anisotropic optical scattering which enabled facile tracking in native tissue using polarization-sensitive

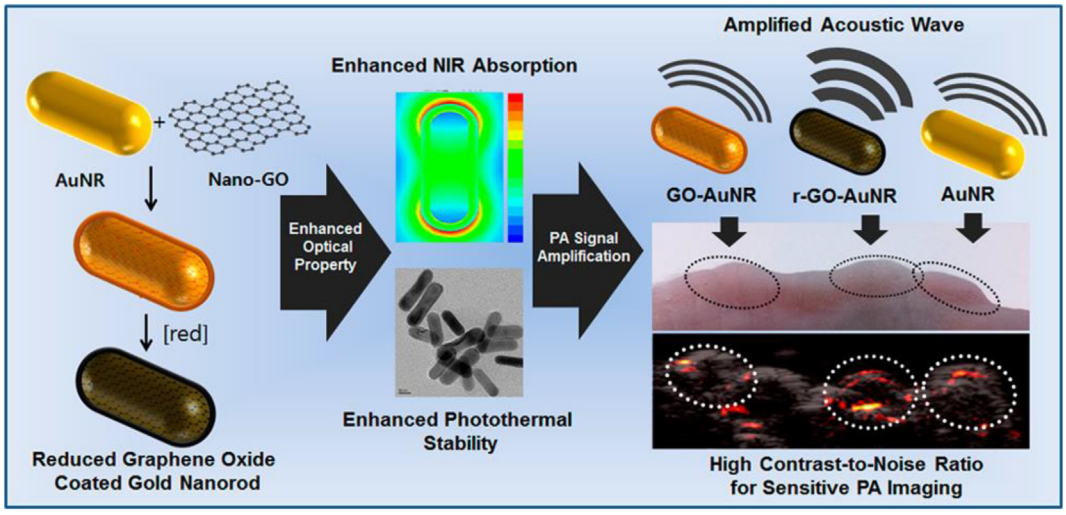

Fig. 5. Photoacoustic (PA) imaging with light-responsive NPs. Graphene-oxide-coated gold nanorods with enhanced NIR absorption and photothermal stability. Reproduced with permission from [19].

OCT [24]. When small nanorods are located in matrix, their Brownian movement is changed by the intermittent collision with neighboring macromolecules. By detecting the polarized light scattering, OCT can reveal the nanotopology of the tissue by noninvasively determining the translational diffusion coefficient (D_T) of the nanorods: increased collagen and cell density resulted in a decreased D_T of the gold nanorods [24]. In the subsequent paper, as shown in Fig. 7, they used gold nanorod-based OCT to monitor the results of pulmonary disease treatment [25]. High solid concentration of pulmonary mucus is a common symptom in respiratory diseases including chronic obstructive pulmonary disorder and cystic fibrosis, and impaired mucus hydration promotes inflammation, infection, and obstructed airways. To monitor the prognosis of pulmonary disease, human bronchial epithelial cells were prepared on mucociliary transport devices with circular tracks and gold nanorods. After clinical mucus-hydrating therapy or hypertonic saline treatment, mucus mixing, mucus hydration, and cellular secretions were determined by analyzing the D_T of the nanorods with OCT. This study demonstrated the potential of OCT using light-responsive NPs for therapeutic monitoring, which may be used in the body with real-time endoscopic OCT in the near future [25]. Additionally, tumor targetability of gold NPs and tumor microvasculature were monitored by OCT [86]. PEGylated gold nanorods were accumulated into the tumor site over time in 4 T1 tumor mice, and the spatial frequency analysis of OCT signals represented tumor vasculature intraoperatively. This study demonstrated that OCT could help monitoring of the therapeutic behaviors of nanomedicine in real time.

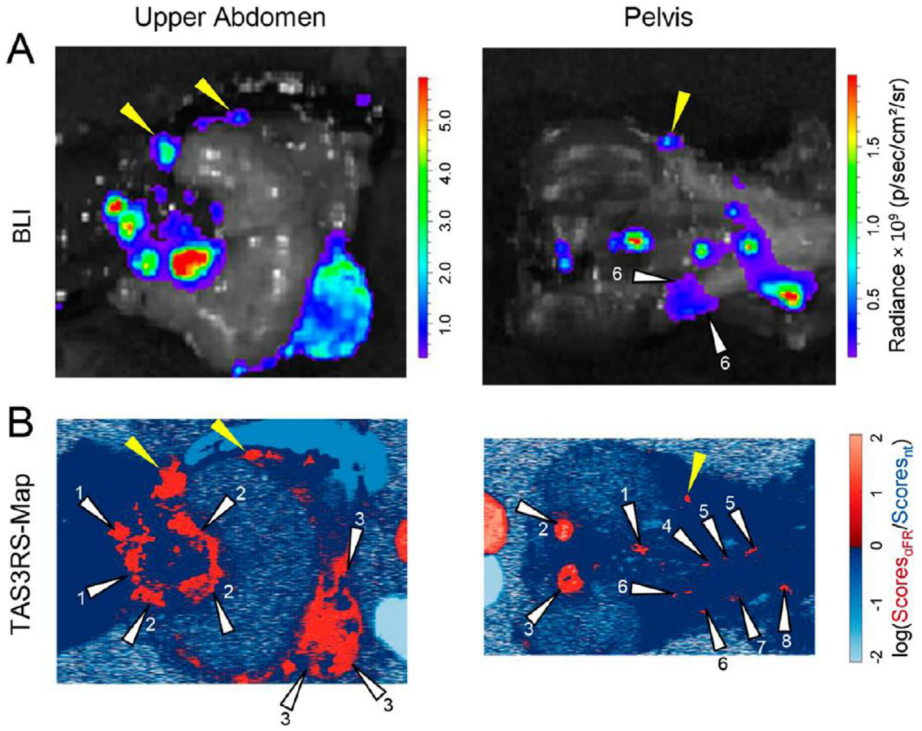

Fig. 6. Surface-enhanced Raman scattering (SERS) with light-responsive NPs. Silica-coated gold nanostars for enhanced Raman signals: (A) Bioluminescence (SKOV-3 cells transfected with luciferase) and (B) TAS3RS (topically applied surface-enhanced resonance Raman ratiometric spectroscopy) map of mice after intraperitoneal injection of nanostars and ratiometric analysis. Reproduced with permission from [23].

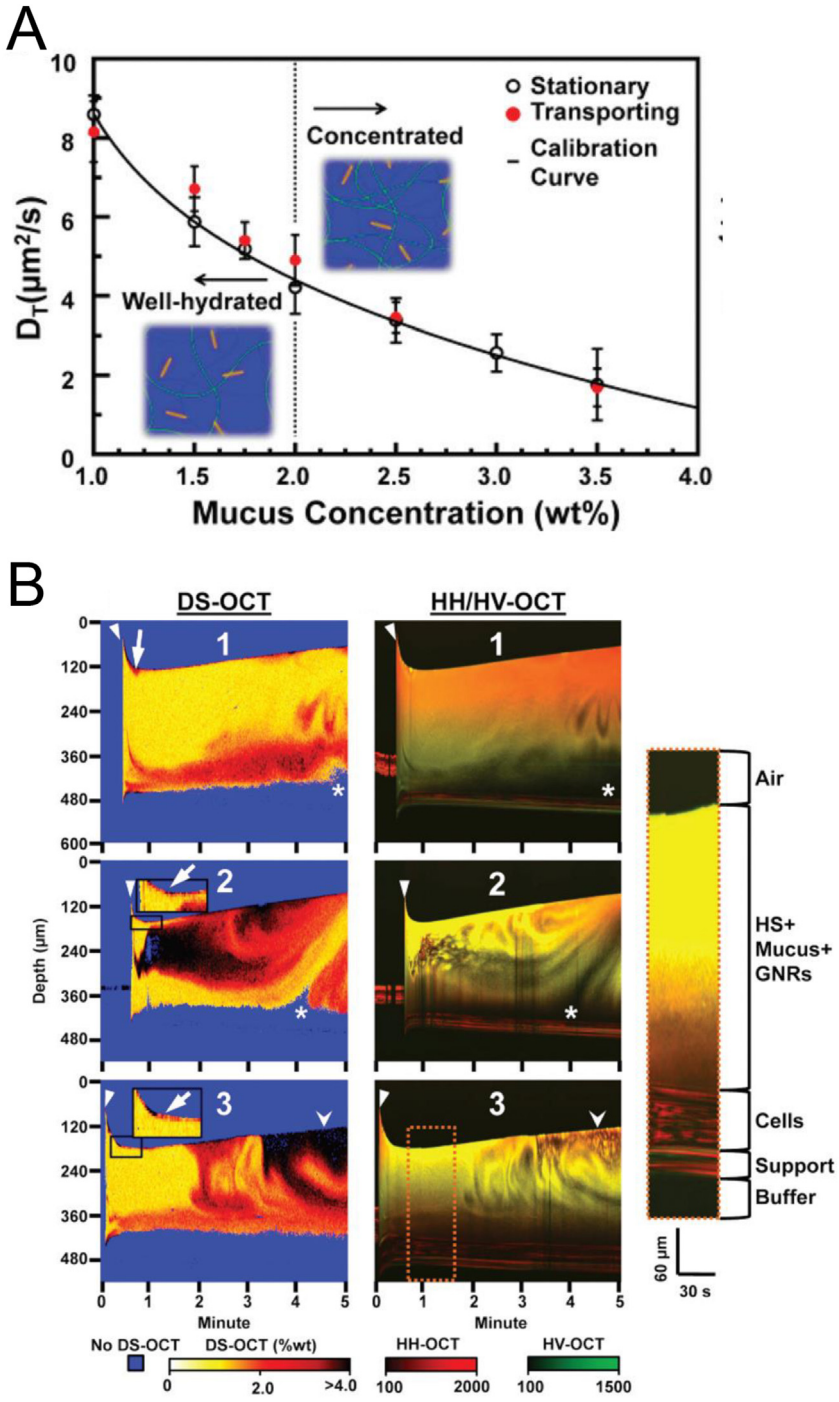

Fig. 7. Optical coherence tomography (OCT) with light-responsive NPs. Gold nanorods for probing nanotopology: (A) Changes in the diffusion of gold nanorods in varied concentrations of mucus. (B) Diffusion sensitive (DS), HH (horizontal in and horizontal out), and HV HH (horizontal in and vertical out) OCT data from nanorod-containing mucus after treatment of isotonic saline. Reproduced with permission from [25].

4. Light-responsive nanomedicine for targeted therapy and drug delivery

Targeting is the key step for improving tissue-specific drug delivery and therapeutic efficacy, which is mainly dependent on the physicochemical properties of targeted agents (*i.e.*, structure-inherent targeting) [87]. After successful targeting, photochemistry can produce toxic molecules for PDT or generate heat for PTT, which enables a controlled release of drugs in the target disease site upon light irradiation. Thus, light-responsive nanomaterials play a pivotal role in these therapeutic applications.

4.1. Photodynamic therapy (PDT)

PDT is a clinical treatment using PS that generates toxic ROS in response to light irradiation (see Section 2.1). PDT has been used solely or in combination with chemotherapy for the treatment of cancers in prostate, skin, head and neck, or colon. PDT is effective in killing

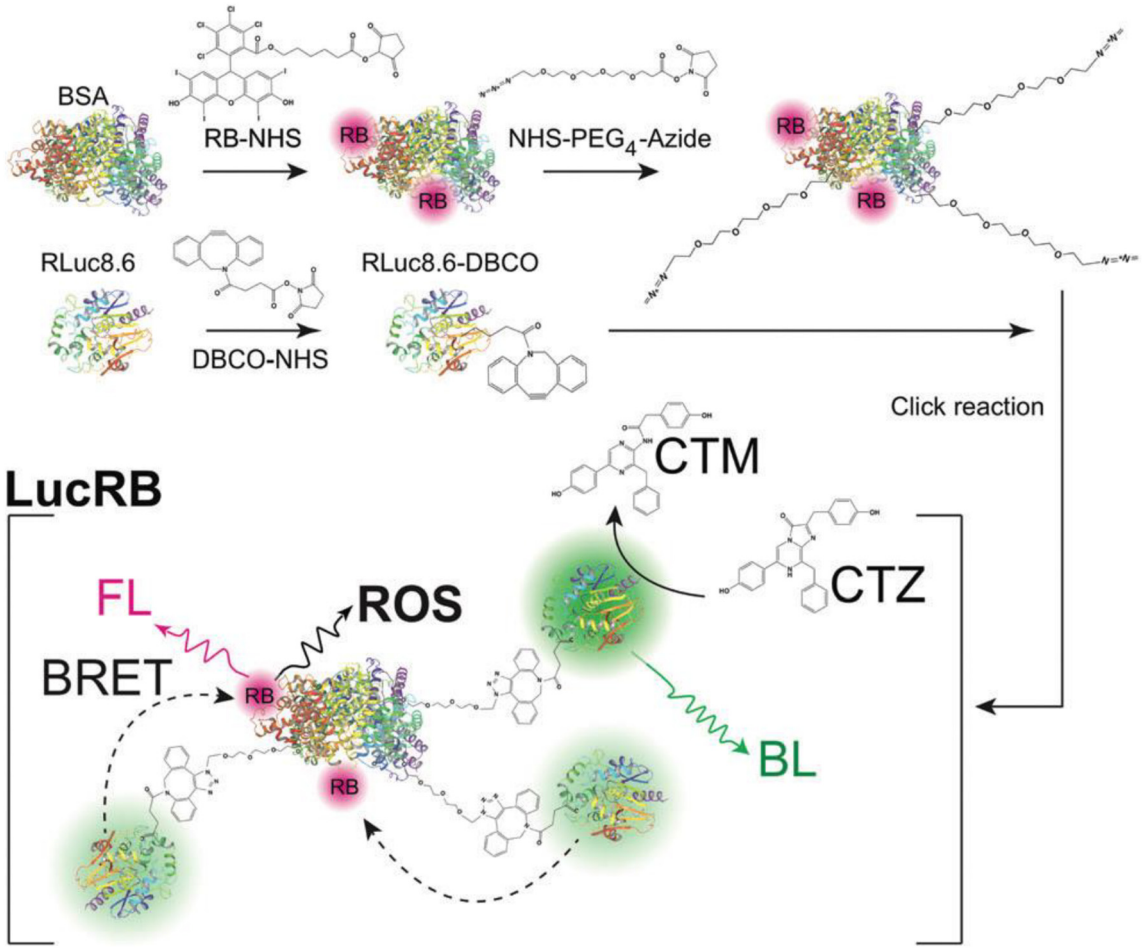

Fig. 8. Photodynamic therapy (PDT) with light-responsive NPs. Bioluminescence-based PDT without external light excitation. Reproduced with permission from [26].

multi-drug-resistant cancer cells after repetitive treatments with chemical drugs, resulting in no cross-resistance with traditional chemotherapy. Easy control of the therapeutic effect by light irradiation is also advantageous. However, PDT is only suitable for tumor tissue where light can reach, and unintended phototoxicity can occur in normal tissue due to the nonspecific accumulation of PSs.

To overcome the light penetration depth issue (see Section 3.1), Kim et al. focused on bioluminescence that is based on the light generating reaction between luciferase and its substrate without any excitation light [26]. As shown in Fig. 8, they developed a bioluminescence resonance energy transfer (BRET) system with luciferase donors and PS acceptors for PDT. For BRET pairs, they selected renilla luciferase 8.6 (RLuc8.6) with an emission peak at 535 nm and rose bengal (RB) with an absorption peak at 550 nm. They prepared RB-conjugated bovine serum albumin and further modified it with multiple RLuc8.6 molecules *via* PEG linkers using copper-free click chemistry. This rationally designed LucRB provided optimal space between RB and RLuc8.6 to avoid quenching and improve BRET efficiency. Coelenterazine (CTZ) was used as the substrate for RLuc8.6, and the LucRB conjugate generated ROS in reaction with CTZ. In addition, a cell-penetrating peptide was noncovalently coupled to LucRB to enhance cellular uptake. Consequently, LucRB successfully killed CT26 murine colon carcinoma cells after treatment with CTZ demonstrating BRET-based PDT without light irradiation. This is a novel strategy to overcome the limitation of traditional PDT, however, its clinical translation will be more challenging because it needs to be proved first that luciferase and luciferin have no harmful effect inside the body.

Another way to improve PDT efficacy is the use of two-photon lasers to provide improved penetration depth and spatial selectivity because nonlinear absorption of the two relatively low-energy photons of NIR light with minimum tissue interference. Initially, two-photon PDT was performed with the combination of nanosecond pulse lasers and porphyrin PSs [88]. This was enabled by the femtosecond NIR lasers developed in the 1990's, which improved two-photon PDT. Organic two-photon PSs were developed by using donor/acceptor groups in their chemical structure with extended π-conjugation. In addition, the use of transitional metal complexes could provide efficient singlet to triplet intersystem crossing by the heavy atom effect. In 2017, Gu et al. developed efficient two-photon absorption PS NPs based on aggregation induced emission (AIE) for PDT [27]. Since most PSs including porphyrin derivatives aggregate easily in aqueous media due to their hydrophobic and rigid planar structures, which cause self-quenching that significantly reduces PDT efficiency. Using tetraphenylethylenes NPs with AIE, the PS ability could be improved in NPs with showing large two-photon absorption. Upon two-photon excitation at 800 nm and 15 mW, these NPs showed efficient ROS generation and triggered necrosis of HeLa cells. More importantly, after a single intravenous injection of these NPs in tumor-bearing mice, fine two-photon images could be obtained at a depth of 200 μm. These NPs then enabled selective closure of blood vessels by PDT in the brain for 4 min demonstrating the advantage of two-photon lasers and efficient two-photon absorbable NPs for targeted PDT [27].

Alternatively, researchers have also been trying to enhance the efficacy of PDT based on its mechanism of action. Generally, fast consumption of oxygen during PDT limits its killing effect, and the hypoxic state in tumor cells or tissues triggers a faster decrease in oxygen concentration. Using this tumor microenvironment, Jia et al. developed manganese (II) oxide-containing NPs which catalyze H_2O_2 to generate

oxygen to improve PDT efficacy [28]. They synthesized carbon dots using a solvothermal process of manganese (II) phthalocyanine and encapsulated them with DSPE-PEG to enhance water solubility and biocompatibility. These NPs showed great anticancer ability in HeLa cells in H_2O_2 – rich and acidic conditions like a tumor microenvironment and demonstrated highly enhanced PDT efficacy in hypoxic tumors. Furthermore, manganese (II) generated from NPs by acidic H_2O_2 is a T1 contrast agent, which is useful for MRI as well as fluorescence imaging enabling theranostic nanomedicine.

Reducing the high glutathione (GSH) levels in cancer cells can also increase the PDT effect because ROS can be reduced by GSH. In 2018, Zhang et al. used nanometal-organic frameworks (MOFs) composed of Cu^{II} and porphyrin derivatives to reduce GSH levels and enhance PDT efficacy [29]. Cu^{II} in MOF can bind to GSH in cancer cells and decrease intracellular GSH levels. Combined with anticancer drugs, MOF showed enhanced therapeutic efficiency showing strong inhibition of tumor growth by PDT upon laser exposure at 650 nm in tumor-bearing mice.

4.2. Photothermal therapy (PTT)

PTT is based on hyperthermia and uses the light-responsive thermal effects of semiconducting polymers, carbon materials, gold, or other metal NPs. To minimize injury to normal tissue, increasing the efficacy of the photothermal effect is highly important, and the specific tissue should be clearly targeted without background uptake [9]. For example, Nam et al. developed polydopamine-coated spiky gold nanoparticles (PDA-SGNP) with high stability and efficiency for combination therapy [30]. As shown in Fig. 9, citrate-stabilized spherical gold NPs were grown to a spiky structure using a surfactant-free method with $AgNO_3$ and ascorbic acid. They were surface-passivated with thiolated PEG chains and further coated using spontaneous polymerization of PDA. The PDA shell endowed strong photothermal stability to SGNPs under extreme heating conditions (> 90 °C), which enabled efficient PTT without deformation to different structures with a low photothermal effect. These PDA-SGNPs showed an enhanced killing effect in CT26 colon cancer cells in a tumor-bearing mice model, where 3 °C higher intratumoral temperatures resulted in more efficient PTT than the uncoated SGNPs. Encouraged by these results, PDA-SGNPs were applied to a more advanced tumor model, highly aggressive TC-1 submucosa-lung tumor. In combination with doxorubicin-based chemotherapy, PDA-SGNPs completely inhibited tumor growth by PTT in the tumor-bearing mice 20 d after tumor inoculation [30].

Separately, using semiconducting polymeric NPs, Wang et al. developed 2D ultrathin PPy nanosheets rather than a simple sphere structure to promote photothermal conversion efficiency [31]. PPy monomers were injected between iron oxychloride template layers and the template was then removed by acid washing to obtain PPy nanosheets with thicknesses of 1–2 nm. The ultrathin planar structure of PPy can cause polaron and bipolaron bands to appear in the band gap as the doping level increases. It resulted in strong absorbance in the second NIR region (1000–1350 nm), which could provide increased tissue penetration due to weak photon scattering in tissue. The synthesized PPy nanosheets were also coated with DSPE-PEG to allow for stable physiological dispersion. Irradiation of the PPy nanosheets (4 mg/kg) injected into MDA-MB-231 breast cancer-bearing mice with a 1064 nm laser (1 W/cm^2) completely inhibited tumor growth by deep tissue PTT [31].

Recently, Gao et al. demonstrated new potential for PTT based on NPs in the treatment of atherosclerosis [32]. During atherosclerosis, vascular smooth muscle cells (VSMCs) as well as monocytes and macrophages accumulate cholesterol and triglycerides to promote the formation of foam cells. Transient receptor potential vanilloid subfamily 1 (TRPV1) is a thermosensitive cation channel, which can induce autophagy in VSMCs and prevent the formation of foam cells. NIR light was used to activate the TRPV1 channel by PTT as well as to generate a PA signal in synthesized CuS NPs. The resulting TRPV1 CuS NPs bound TRPV1 channels on VSMCs and increased intracellular Ca^{2+} concentrations by photothermal effect when exposed to an NIR laser. Intravenous administration of these NPs (10 mg/ml) in the plaque-bearing $ApoE^{-/-}$ mice resulted in an increased PA signal over time in the aortic arch region due to the EPR-based targeting. NIR laser irradiation in the cardiac region for 30 cycles twice a week resulted in improved TRPV1 activation and a therapeutic effect by PTT [32].

On the other hand, Zhou et al. suggested that low-temperature PTT would be an effective combinational therapy with PTT using a tumor-

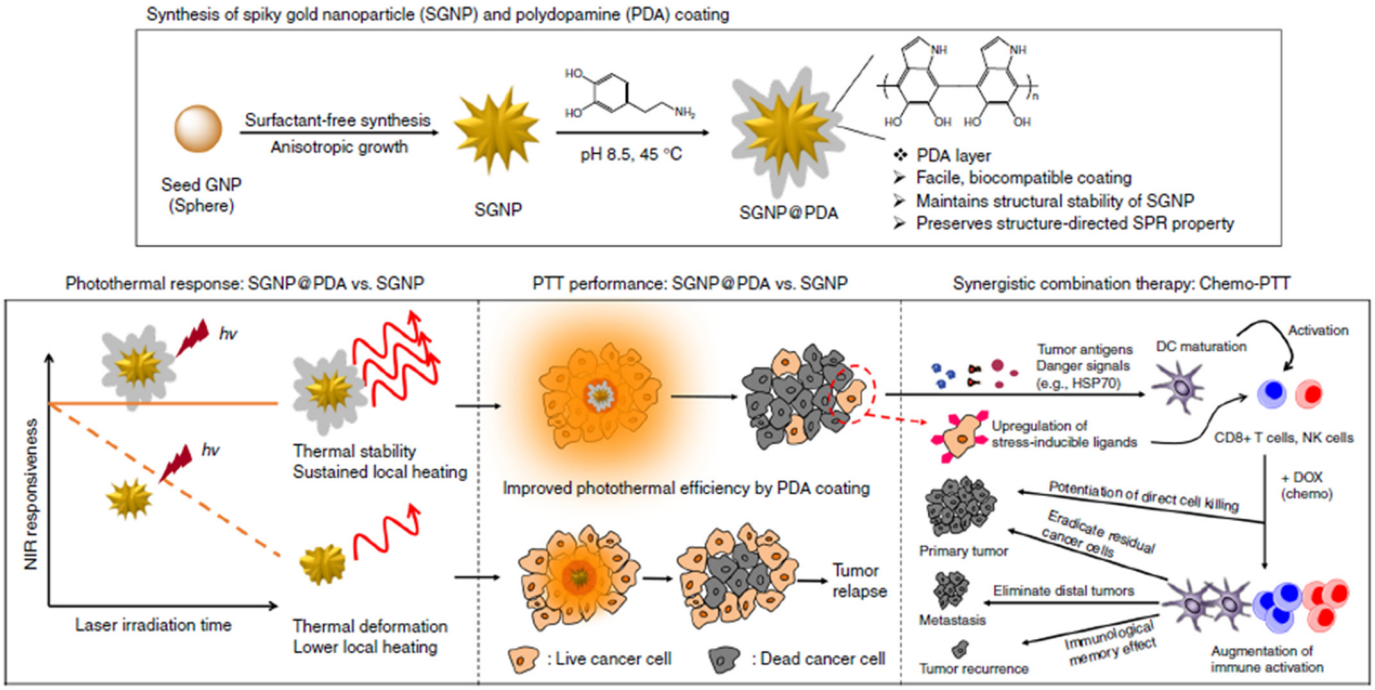

Fig. 9. Photothermal therapy (PTT) with light-responsive NPs. Polydopamine-coated spiked gold NPs with improved photothermal effect and photo-stability. Reproduced with permission from [30].

targeted redox-responsive nanoplatform [33]. This system uses porous hollow Prussian blue NPs (PHPBNs) that have catalase-like activity to catalyze the decomposition of H_2O_2 in tumors for reoxygenation. Glucose oxidase (GOx) was loaded at the center of the PHPBNs, and hyaluronic acid (HA) was coated onto the surface to target CD44 receptors on tumor cells. GOx can consume glucose resulting in tumor starvation and the generated H_2O_2 can be turned into oxygen and water by PHPBNs. In addition, these NPs have a high absorption coefficient ranging from 500 to 900 nm (centered at 780 nm), and they reached a temperature exceeding 60 °C after irradiation with a NIR laser (808 nm, 1 W/cm^2) for 5 min. They showed fast cellular uptake and a killing effect in HepG2 human liver cancer cells with overexpressed CD44 receptors; these effects were also achieved in HepG2 tumor-bearing mice using 808 nm laser irradiation 24 h post-injection. The maximum temperature of the tumor was only 45 °C after irradiation, but these NPs effectively suppressed tumor growth in multiple combination strategies based on tumor starvation and PTT [33].

4.3. Light-responsive drug delivery

Light-responsive NPs are useful for photo-triggered drug release upon irradiation, which generally uses photo-degradable chemical bonds, photothermal effect-induced structural changes, or a photo-induced decrease in hydrophobicity [89]. These strategies enable stable storage of drugs in NPs during blood circulation and controlled drug release only in the target tissue upon light irradiation [83,90]. Rwei et al. fabricated NIR light-triggered liposomes, resulting in controlled drug release upon irradiation [34]. They loaded hydrophilic tetrodotoxin (TTX), a local anesthetic, into the inner empty portion of liposomes and also encapsulated hydrophobic palladium PS within the bilayer shell membrane. Upon NIR irradiation, PS produced a singlet oxygen, which could lead to peroxidation of unsaturated lipid, formation of an α-bond, and a 1,5 hydrogen shift. This phenomenon makes lipids hydrophilic, thereby destabilizing the lipid layer and allowing drug release. The ROS-reactive lipid caused an initial nerve block for over 12 h because of its high reactivity with ROS. The results demonstrated that light-responsive liposomes are useful in patients where the timing, intensity, and duration of local anesthesia need to be controlled [34]. In the subsequent paper, they prepared low temperature-sensitive liposomes using TTX-loaded phosphocholine in the nanorod [35]. The surface had gold nanorods designed for streptavidin-biotin binding. When exposed to NIR light (808 nm), the gold nanorods generated heat and induced a phase transition in the lipid membrane resulting in rapid release of the encapsulated TTX. Without irradiation, the liposomes exhibited sustained release at 37 °C. NIR light irradiation can be an efficient tool to trigger drug release, but high and prolong irradiation may cause side effect such as burns. This system effectively triggered a sciatic nerve block *in vivo* with NIR irradiation for 1–2 min at 272 mW/cm^2, very short duration time and low irradiance [35].

The Zheng group is a pioneer in renal clearable gold NPs [91–94]. Renal clearable ultrasmall gold NPs can be used for passive tumor targeting based on their rapid biodistribution and sustained retention at the tumor microenvironment. Especially, gold NPs are advantageous for quantification of renal transport kinetics and tumor targeting when combined with NIR and X-ray imaging modality [77]. Indeed, selective delivery of nanomedicine to the tumor site is vital to minimizing the potential toxicity of NPs and expediting their clinical translation [11]. Since solid tumors often exhibit unique microenvironments such as leaky microvasculature and impaired lymphatic drainage as well as acidic extracellular pH (pH ≈ 6.5), which can be of great target for enhancing drug delivery using ultrasmall gold NPs through the EPR effect [58].

Hasan et al. designed a lipid bilayer of liposome containing PSs and drugs, which can release incorporated materials triggered by NIR light followed by breakdown of liposome structure [37]. They synthesized photoactivable multi-inhibitor nanoliposomes (PMIL) for photoinitiated and sustained release of inhibitors. The PMIL contains benzoporphyrin derivatives (BPD) as the PS in the lipid bilayer and smaller polymeric NPs loaded with cabozantinib (XL184), a multikinase inhibitor, in the NP core. NIR light activated BPD, broke the liposome bilayer, and increased the release rate of XL184 from PMIL. The released XL184 inhibited vascular endothelial growth factor (VEGF) signaling in the tumor microvasculature, thereby inducing suppression of tumor angiogenesis and vascular regrowth after PDT. Furthermore, XL184 inhibits MET signaling which controls tumor cell motility, invasion and metastasis. Photo-initiated release of XL184 and PDT using PMIL showed an efficient reduction of tumor growth in an AsPC1 tumor bearing mouse model based on photothermal and multikinase inhibition effects. Furthermore, PMIL also decreased metastasis to the liver and retroperitoneal lymph node, and reduced intratumoral microvessel growth in orthotopic pancreatic tumor models [37].

Alternatively, Pei et al. utilized a chemical bond which is cleavable by generated ROS after PDT [38]. As shown Fig. 10, they synthesized a ROS-sensitive paclitaxel dimer (PTX_2-TK) with a thioketal (TK) linker which allowed for rapid release of PTX upon interaction with ROS. PTX_2-TK and 5,10,15,20-tetraphenylchlorin (TPC) as the PS were loaded into red blood cell (RBC) membrane-camouflaged NPs. This erythrocyte membrane reduced uptake by macrophages and provided long blood circulation similar to natural RBCs. The resulting RBC(M(TPC-PTX)) efficiently generated ROS from TPC upon laser irradiation and the generated ROS also broke the TK linker in PTX_2-TK, allowing for PTX release. This system could prevent unintended drug release during blood circulation. After a single intravenous injection of RBC(M(TPC-PTX)) into HeLa tumor-bearing nude mice, sustained blood circulation, high tumor uptake, and effective therapeutic results with no other side effect were observed. These NPs demonstrated high biocompatibility, on-demand drug release, and a synergetic combination of PDT and chemotherapy therapy [38].

5. Conclusions and perspectives

In this review, we discussed many types of light-responsive NPs and their biomedical applications: biophotonic imaging, including luminescence imaging, PA, SERS, and OCT, as well as targeted therapies such as PDT, PTT, and light-responsive drug delivery. Despite of the great promise of NPs proven in preclinical research, there are also some critical challenges we need to consider for their clinical translation: First, most activities using these NPs either for imaging or therapy are not free from the intrinsic limitations of light in living organisms. The limited penetration depth of light into tissue is the foremost representative disadvantage of using these light-responsive NPs [3]. This can be partially overcome by 1) increasing the sensitivity to light using chemical modification of NPs; 2) decreasing background signals using low-power excitation in the NIR window; 3) decreasing background signals using ultrasmall NPs to eliminate unbound molecules from the body; and 3) lowering tissue scattering of NPs in the NIR-1b and NIR-II window (900–1700 nm). Nevertheless, these approaches cannot completely solve the penetration depth issue, and multimodal approaches using NIR-nuclear imaging or NIR-MRI will be helpful [95]. Second, most light-induced treatments require knowing the exact site of irradiation. This represents a critical limitation that many clinical cases require targeting unknown disease tissues or cells. Of course, a recent technique for PDT based on bioluminescence has promising potential [26]. Fundamentally, however, more accurate targeting of multifunctional NPs to the specific tissue will be required to resolve this issue [8,9].

Furthermore, although not discussed in depth in this review, establishing reproducible synthesis procedures and scale-up processes of NPs for commercial translation is a significant challenge. The scale-up chemistry of inorganic NPs is relatively easier due to the crystal growing process from atoms [57], while it has been a challenge for organic NPs [79]. Among many trials, automated layer-by-layer templating with agarose-suspended templates significantly improved the scale-up

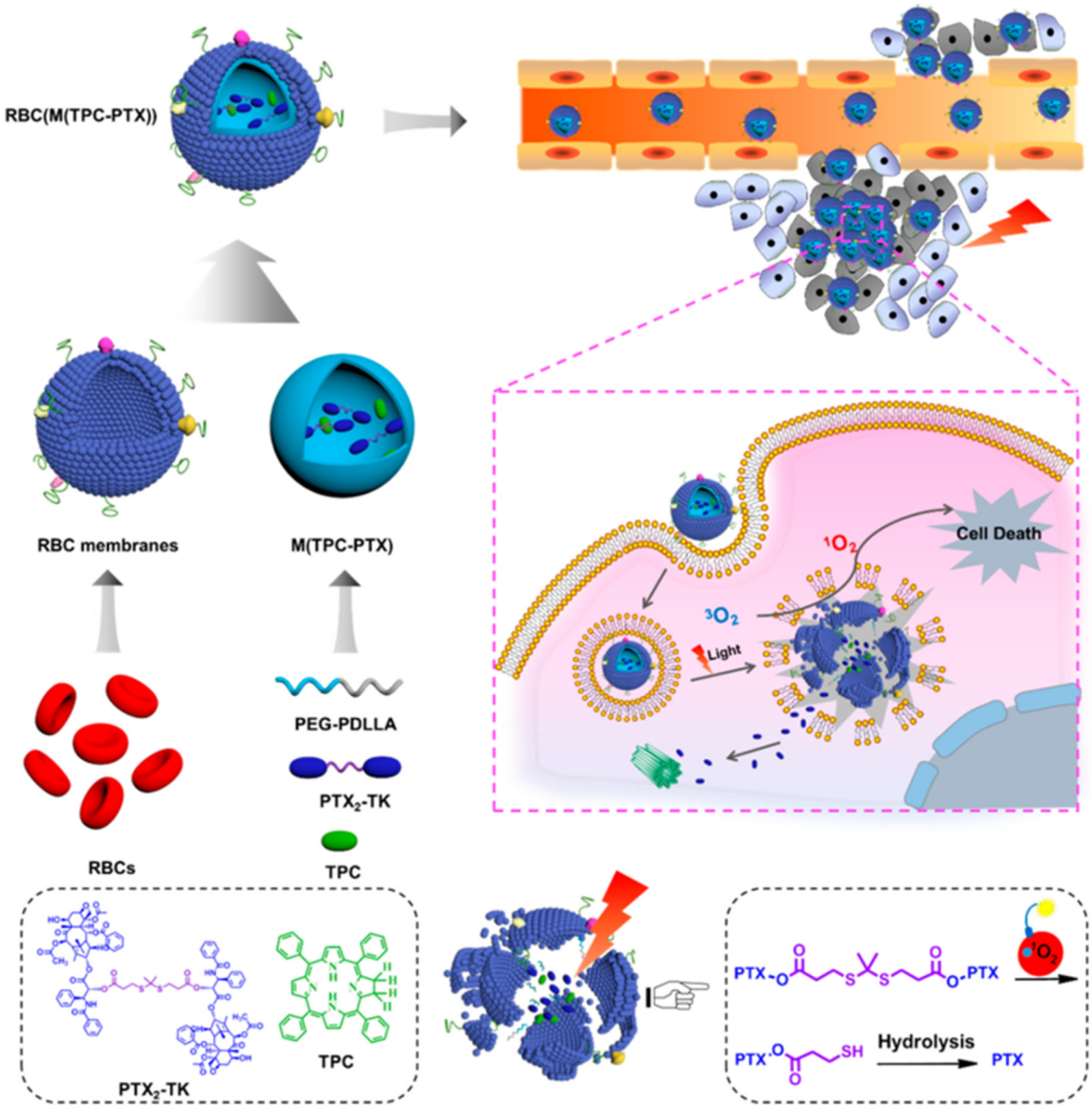

Fig. 10. Light-responsive drug delivery with light-responsive NPs. Reactive oxygen species (ROS) triggered drug release in combination therapy. Reproduced with permission from [38].

process of NPs [96]. Additionally, particle replication in non-wetting templates (PRINT) could also synthesize polymeric NPs with different physicochemical properties by a top-down lithographic method [97]. Successful scale-up of NPs with controllable reproducibility is crucial for commercialization of light-responsive NPs considering the cost and quality control [79], which must be researched in detail.

Besides of increasing efficiency and scale-up synthesis, to be clinically available, these NPs should not result in any toxicity and need to get FDA approval before human use. For these reasons, the "Choi Criteria" should be the first and foremost important design considerations for clinically applicable NPs (reviewed in [8]): First, the components of NPs need to be selected from among nontoxic molecules and/or biodegradable components. Natural materials or FDA-approved molecules are good candidates, and organic materials are relatively advantageous over inorganic ones in this context [18]. Second, the surface charge of the NPs should be considered to minimize cellular interactions with normal tissue and thereby avoid nonspecific uptake. Serum protein binding is the first challengeable interaction that systemically administered NPs would face in the body. Finally, rapid elimination of unbound NPs from the body also needs to be considered carefully. The size and shape of NPs along with their surface charges are the key modulators for renal *vs.* hepatobiliary elimination of unbound molecules after targeting. In this regard, an HD of 5.5 nm is the critical threshold for NPs to result in rapid renal clearance [7,36]. Without considering such fundamental limitations, NPs will eventually encounter prohibitive regulatory hurdles and there will be very limited clinical applications due to the potential toxicity.

Acknowledgments

We thank Ivey Choi for manuscript editing. This study was supported by the Basic Science Research Program of the National Research Foundation of Korea (NRF) funded by the Ministry of Education, South Korea (grant no. 2016R1C1B3013951) and the US NIH grant NIBIB #R01-EB022230.

References

[1] R. Weissleder, A clearer vision for in vivo imaging, Nat. Biotechnol. 19 (2001) 316–317.
[2] X. Shu, A. Royant, M.Z. Lin, T.A. Aguilera, V. Lev-Ram, P.A. Steinbach, R.Y. Tsien, Mammalian expression of infrared fluorescent proteins engineered from a bacterial phytochrome, Science 324 (2009) 804–807.

[3] E.A. Owens, S. Lee, J. Choi, M. Henary, H.S. Choi, NIR fluorescent small molecules for intraoperative imaging, Wiley Interdiscip Rev Nanomed Nanobiotechnol 7 (2015) 828–838.
[4] Q. Zubair, H.Y. Mohamed, Role of ultraviolet (UV) disinfection in infection control and environmental cleaning, Infectious Disorders - Drug Targets 13 (2013) 191–195.
[5] P. Weis, S. Wu, Light-switchable azobenzene-containing macromolecules: from UV to near infrared, Macromol. Rapid Commun. 39 (2018), 1700220.
[6] C.A. Deforest, K.S. Anseth, Cytocompatible click-based hydrogels with dynamically tunable properties through orthogonal photoconjugation and photocleavage reactions, Nat. Chem. 3 (2011) 925–931.
[7] K. Bao, K.A. Nasr, H. Hyun, J.H. Lee, J. Gravier, S.L. Gibbs, H.S. Choi, Charge and hydrophobicity effects of NIR fluorophores on bone-specific imaging, Theranostics 5 (2015) 609–617.
[8] H.S. Choi, J.V. Frangioni, Nanoparticles for biomedical imaging: fundamentals of clinical translation, Mol. Imaging 9 (2010) 291–310.
[9] E.A. Owens, M. Henary, G. El Fakhri, H.S. Choi, Tissue-specific near-infrared fluorescence imaging, Acc. Chem. Res. 49 (2016) 1731–1740.
[10] A.C. Anselmo, S. Mitragotri, Nanoparticles in the clinic, Bioeng Transl Med 1 (2016) 10–29.
[11] J.H. Lee, G. Park, G.H. Hong, J. Choi, H.S. Choi, Design considerations for targeted optical contrast agents, Quant Imaging Med Surg 2 (2012) 266–273.
[12] G.K. Park, H. I, G.S. Kim, N.S. Hwang, H.S. Choi, Optical spectroscopic imaging for cell therapy and tissue engineering, Appl. Spectrosc. Rev. 53 (2018) 360–375.
[13] S. Dufort, L. Sancey, J.L. Coll, Physico-chemical parameters that govern nanoparticles fate also dictate rules for their molecular evolution, Adv. Drug Deliv. Rev. 64 (2012) 179–189.
[14] X. Yue, Q. Zhang, Z. Dai, Near-infrared light-activatable polymeric nanoformulations for combined therapy and imaging of cancer, Adv. Drug Deliv. Rev. 115 (2017) 155–170.
[15] J. Park, M. Xu, F. Li, H.-C. Zhou, 3D long-range triplet migration in a water-stable metal–organic framework for upconversion-based ultralow-power in vivo imaging, J. Am. Chem. Soc. 140 (2018) 5493–5499.
[16] Y.I. Park, H.M. Kim, J.H. Kim, K.C. Moon, B. Yoo, K.T. Lee, N. Lee, Y. Choi, W. Park, D. Ling, K. Na, W.K. Moon, S.H. Choi, H.S. Park, S.-Y. Yoon, Y.D. Suh, S.H. Lee, T. Hyeon, Theranostic probe based on lanthanide-doped nanoparticles for simultaneous in vivo dual-modal imaging and photodynamic therapy, Adv. Mater. 24 (2012) 5755–5761.
[17] J. Wang, Q. Ma, X.-X. Hu, H. Liu, W. Zheng, X. Chen, Q. Yuan, W. Tan, Autofluorescence-free targeted tumor imaging based on luminous nanoparticles with composition-dependent size and persistent luminescence, ACS Nano 11 (2017) 8010–8017.
[18] H. Kang, J. Gravier, K. Bao, H. Wada, J.H. Lee, Y. Baek, G. El Fakhri, S. Gioux, B.P. Rubin, J.-L. Coll, H.S. Choi, Renal clearable organic nanocarriers for bioimaging and drug delivery, Adv. Mater. 28 (2016) 8162–8168.
[19] H. Moon, D. Kumar, H. Kim, C. Sim, J.-H. Chang, J.-M. Kim, H. Kim, D.-K. Lim, Amplified photoacoustic performance and enhanced photothermal stability of reduced graphene oxide coated gold nanorods for sensitive photoacoustic imaging, ACS Nano 9 (2015) 2711–2719.
[20] C. Xie, X. Zhen, Y. Lyu, K. Pu, Nanoparticle regrowth enhances photoacoustic signals of semiconducting macromolecular probe for in vivo imaging, Adv. Mater. 29 (2017), 1703693.
[21] Z. Yang, R. Tian, J. Wu, Q. Fan, B.C. Yung, G. Niu, O. Jacobson, Z. Wang, G. Liu, G. Yu, W. Huang, J. Song, X. Chen, Impact of semiconducting perylene diimide nanoparticle size on lymph node mapping and cancer imaging, ACS Nano 11 (2017) 4247–4255.
[22] S. Harmsen, R. Huang, M.A. Wall, H. Karabeber, J.M. Samii, M. Spaliviero, J.R. White, S. Monette, R. O'Connor, K.L. Pitter, S.A. Sastra, M. Saborowski, E.C. Holland, S. Singer, K. P. Olive, S.W. Lowe, R.G. Blasberg, M.F. Kircher, Surface-enhanced resonance Raman scattering nanostars for high-precision cancer imaging, Sci. Transl. Med. 7 (2015) 271ra277.
[23] A. Oseledchyk, C. Andreou, M.A. Wall, M.F. Kircher, Folate-targeted surface-enhanced resonance Raman scattering nanoprobe ratiometry for detection of microscopic ovarian cancer, ACS Nano 11 (2017) 1488–1497.
[24] R.K. Chhetri, R.L. Blackmon, W.-C. Wu, D.B. Hill, B. Button, P. Casbas-Hernandez, M.A. Troester, J.B. Tracy, A.L. Oldenburg, Probing biological nanotopology via diffusion of weakly constrained plasmonic nanorods with optical coherence tomography, Proc. Natl. Acad. Sci. 111 (2014) E4289–E4297.
[25] R.L. Blackmon, S.M. Kreda, P.R. Sears, B.S. Chapman, D.B. Hill, J.B. Tracy, L.E. Ostrowski, A.L. Oldenburg, Direct monitoring of pulmonary disease treatment biomarkers using plasmonic gold nanorods with diffusion-sensitive OCT, Nanoscale 9 (2017) 4907–4917.
[26] S. Kim, H. Jo, M. Jeon, M.-G. Choi, S.K. Hahn, S.-H. Yun, Luciferase-Rose Bengal conjugates for singlet oxygen generation by bioluminescence resonance energy transfer, Chem. Commun. 53 (2017) 4569–4572.
[27] B. Gu, W. Wu, G. Xu, G. Feng, F. Yin, P.H.J. Chong, J. Qu, K.-T. Yong, B. Liu, Precise two-photon photodynamic therapy using an efficient photosensitizer with aggregation-induced emission characteristics, Adv. Mater. 29 (2017), 1701076.
[28] Q. Jia, J. Ge, W. Liu, X. Zheng, S. Chen, Y. Wen, H. Zhang, P. Wang, A magnetofluorescent carbon dot assembly as an acidic H_2O_2-driven oxygenerator to regulate tumor hypoxia for simultaneous bimodal imaging and enhanced photodynamic therapy, Adv. Mater. 30 (2018) 1706090.
[29] W. Zhang, J. Lu, X. Gao, P. Li, W. Zhang, Y. Ma, H. Wang, B. Tang, Enhanced photodynamic therapy by reduced levels of intracellular glutathione obtained by employing a nano-MOF with CuII as the active center, Angew. Chem. Int. Ed. 57 (2018) 4891–4896.
[30] J. Nam, S. Son, L.J. Ochyl, R. Kuai, A. Schwendeman, J.J. Moon, Chemo-photothermal therapy combination elicits anti-tumor immunity against advanced metastatic cancer, Nat. Commun. 9 (2018) 1074.
[31] X. Wang, Y. Ma, X. Sheng, Y. Wang, H. Xu, Ultrathin polypyrrole nanosheets via space-confined synthesis for efficient photothermal therapy in the second near-infrared window, Nano Lett. 18 (2018) 2217–2225.
[32] W. Gao, Y. Sun, M. Cai, Y. Zhao, W. Cao, Z. Liu, G. Cui, B. Tang, Copper sulfide nanoparticles as a photothermal switch for TRPV1 signaling to attenuate atherosclerosis, Nat. Commun. 9 (2018) 231.
[33] J. Zhou, M. Li, Y. Hou, Z. Luo, Q. Chen, H. Cao, R. Huo, C. Xue, L. Sutrisno, L. Hao, Y. Cao, H. Ran, L. Lu, K. Li, K. Cai, Engineering of a nanosized biocatalyst for combined tumor starvation and low-temperature photothermal therapy, ACS Nano 12 (2018) 2858–2872.
[34] A.Y. Rwei, J.-J. Lee, C. Zhan, Q. Liu, M.T. Ok, S.A. Shankarappa, R. Langer, D.S. Kohane, Repeatable and adjustable on-demand sciatic nerve block with phototriggerable liposomes, Proc. Natl. Acad. Sci. 112 (2015), 15719.
[35] C. Zhan, W. Wang, C. Santamaria, B. Wang, A. Rwei, B.P. Timko, D.S. Kohane, Ultrasensitive phototriggered local anesthesia, Nano Lett. 17 (2017) 660–665.
[36] J. Xu, C. Peng, M. Yu, J. Zheng, Renal clearable noble metal nanoparticles: photoluminescence, elimination, and biomedical applications, Wiley Interdiscip Rev Nanomed Nanobiotechnol 9 (2017).
[37] B.Q. Spring, R. Bryan Sears, L.Z. Zheng, Z. Mai, R. Watanabe, M.E. Sherwood, D.A. Schoenfeld, B.W. Pogue, S.P. Pereira, E. Villa, T. Hasan, A photoactivable multi-inhibitor nanoliposome for tumour control and simultaneous inhibition of treatment escape pathways, Nat Nano 11 (2016) 378–387.
[38] Q. Pei, X. Hu, X. Zheng, S. Liu, Y. Li, X. Jing, Z. Xie, Light-activatable red blood cell membrane-camouflaged dimeric prodrug nanoparticles for synergistic photodynamic/chemotherapy, ACS Nano 12 (2018) 1630–1641.
[39] A.M. Bittel, A.M. Davis, L. Wang, M.A. Nederlof, J.O. Escobedo, R.M. Strongin, S.L. Gibbs, Varied length stokes shift BODIPY-based fluorophores for multicolor microscopy, Sci. Rep. 8 (2018) 4590.
[40] H.S. Choi, S.L. Gibbs, J.H. Lee, S.H. Kim, Y. Ashitate, F. Liu, H. Hyun, G. Park, Y. Xie, S. Bae, M. Henary, J.V. Frangioni, Targeted zwitterionic near-infrared fluorophores for improved optical imaging, Nat. Biotechnol. 31 (2013) 148–153.
[41] H.Y. Yoon, H. Koo, K. Kim, I.C. Kwon, Molecular imaging based on metabolic glycoengineering and bioorthogonal click chemistry, Biomaterials 132 (2017) 28–36.
[42] H. Hyun, M. Henary, T. Gao, L. Narayana, E.A. Owens, J.H. Lee, G. Park, H. Wada, Y. Ashitate, J.V. Frangioni, H.S. Choi, 700-nm zwitterionic near-infrared fluorophores for dual-channel image-guided surgery, Mol. Imaging Biol. 18 (2016) 52–61.
[43] K.S. Kim, H. Hyun, J.A. Yang, M.Y. Lee, H. Kim, S.H. Yun, H.S. Choi, S.K. Hahn, Bioimaging of hyaluronate-interferon alpha conjugates using a non-interfering zwitterionic fluorophore, Biomacromolecules 16 (2015) 3054–3061.
[44] K.S. Kim, Y.S. Kim, K. Bao, H. Wada, H.S. Choi, S.K. Hahn, Bioimaging of botulinum toxin and hyaluronate hydrogels using zwitterionic near-infrared fluorophores, Biomater Res 21 (2017) 15.
[45] S.H. Kim, J.H. Lee, H. Hyun, Y. Ashitate, G. Park, K. Robichaud, E. Lunsford, S.J. Lee, G. Khang, H.S. Choi, Near-infrared fluorescence imaging for noninvasive trafficking of scaffold degradation, Sci. Rep. 3 (2013) 1198.
[46] H. Wada, H. Hyun, K. Bao, J.H. Lee, G. El Fakhri, Y. Choi, H.S. Choi, Multivalent mannose-decorated NIR nanoprobes for targeting pan lymph nodes, Chem. Eng. J. 340 (2018) 51–57.
[47] R. Atreya, H. Neumann, C. Neufert, M.J. Waldner, U. Billmeier, Y. Zopf, M. Willma, C. App, T. Munster, H. Kessler, S. Maas, B. Gebhardt, R. Heimke-Brinck, E. Reuter, F. Dorje, T.T. Rau, W. Uter, T.D. Wang, R. Kiesslich, M. Vieth, E. Hannappel, M.F. Neurath, In vivo imaging using fluorescent antibodies to tumor necrosis factor predicts therapeutic response in Crohn's disease, Nat. Med. 20 (2014) 313–318.
[48] S. Lee, J.H. Ryu, K. Park, A. Lee, S.-Y. Lee, I.-C. Youn, C.-H. Ahn, S.M. Yoon, S.-J. Myung, D.H. Moon, X. Chen, K. Choi, I.C. Kwon, K. Kim, Polymeric nanoparticle-based activatable near-infrared nanosensor for protease determination in vivo, Nano Lett. 9 (2009) 4412–4416.
[49] I. Roy, T.Y. Ohulchanskyy, H.E. Pudavar, E.J. Bergey, A.R. Oseroff, J. Morgan, T.J. Dougherty, P.N. Prasad, Ceramic-based nanoparticles entrapping water-insoluble photosensitizing anticancer drugs: a novel drug—carrier system for photodynamic therapy, J. Am. Chem. Soc. 125 (2003) 7860–7865.
[50] M. Mitsunaga, M. Ogawa, N. Kosaka, L.T. Rosenblum, P.L. Choyke, H. Kobayashi, Cancer cell-selective in vivo near infrared photoimmunotherapy targeting specific membrane molecules, Nat. Med. 17 (2011) 1685–1691.
[51] J. Yang, J. Choi, D. Bang, E. Kim, E.-K. Lim, H. Park, J.-S. Suh, K. Lee, K.-H. Yoo, E.-K. Kim, Y.-M. Huh, S. Haam, Convertible organic nanoparticles for near-infrared photothermal ablation of cancer cells, Angew. Chem. Int. Ed. 50 (2011) 441–444.
[52] W. Park, S. Cho, J. Han, H. Shin, K. Na, B. Lee, D.H. Kim, Advanced smart-photosensitizers for more effective cancer treatment, Biomater Sci 6 (2017) 79–90.
[53] R. Verteporfin, i. Participants, Treatment of age-related macular degeneration with photodynamic therapy study group principal, i. Verteporfin in photodynamic therapy study group principal, guidelines for using verteporfin (visudyne) in photodynamic therapy to treat choroidal neovascularization due to age-related macular degeneration and other causes, Retina 22 (2002) 6–18.
[54] K. Yang, S. Zhang, G. Zhang, X. Sun, S.-T. Lee, Z. Liu, Graphene in mice: ultrahigh in vivo tumor uptake and efficient photothermal therapy, Nano Lett. 10 (2010) 3318–3323.
[55] V. Torchilin, Tumor delivery of macromolecular drugs based on the EPR effect, Adv. Drug Deliv. Rev. 63 (2011) 131–135.
[56] S. Gurunathan, J.H. Kim, Synthesis, toxicity, biocompatibility, and biomedical applications of graphene and graphene-related materials, Int. J. Nanomedicine 11 (2016) 1927–1945.
[57] J. Kim, S. Park, J.E. Lee, S.M. Jin, J.H. Lee, I.S. Lee, I. Yang, J.S. Kim, S.K. Kim, M.H. Cho, T. Hyeon, Designed fabrication of multifunctional magnetic gold nanoshells and their

application to magnetic resonance imaging and photothermal therapy, Angew Chem Int Ed Engl 45 (2006) 7754–7758.
[58] J. Liu, M. Yu, C. Zhou, S. Yang, X. Ning, J. Zheng, Passive tumor targeting of renal-clearable luminescent gold nanoparticles: long tumor retention and fast normal tissue clearance, J. Am. Chem. Soc. 135 (2013) 4978–4981.
[59] X. Huang, I.H. El-Sayed, W. Qian, M.A. El-Sayed, Cancer cell imaging and photothermal therapy in the near-infrared region by using gold nanorods, J. Am. Chem. Soc. 128 (2006) 2115–2120.
[60] H.S. Choi, B.I. Ipe, P. Misra, J.H. Lee, M.G. Bawendi, J.V. Frangioni, Tissue- and organ-selective biodistribution of NIR fluorescent quantum dots, Nano Lett. 9 (2009) 2354–2359.
[61] H.S. Choi, W. Liu, F. Liu, K. Nasr, P. Misra, M.G. Bawendi, J.V. Frangioni, Design considerations for tumour-targeted nanoparticles, Nat. Nanotechnol. 5 (2010) 42–47.
[62] H.S. Choi, W. Liu, P. Misra, E. Tanaka, J.P. Zimmer, B. Itty Ipe, M.G. Bawendi, J.V. Frangioni, Renal clearance of quantum dots, Nat. Biotechnol. 25 (2007) 1165–1170.
[63] W. Liu, H.S. Choi, J.P. Zimmer, E. Tanaka, J.V. Frangioni, M. Bawendi, Compact cysteine-coated CdSe(ZnCdS) quantum dots for in vivo applications, J. Am. Chem. Soc. 129 (2007) 14530–14531.
[64] E. Tanaka, H.S. Choi, H. Fujii, M.G. Bawendi, J.V. Frangioni, Image-guided oncologic surgery using invisible light: completed pre-clinical development for sentinel lymph node mapping, Ann. Surg. Oncol. 13 (2006) 1671–1681.
[65] M. Baker, L. Defrancesco, Five more years of nature biotechnology research, Nat Biotech 29 (2011) 221–227.
[66] D. Kim, N. Lee, Y.I. Park, T. Hyeon, Recent advances in inorganic nanoparticle-based NIR luminescence imaging: Semiconductor nanoparticles and lanthanide nanoparticles, Bioconjug. Chem. 28 (2017) 115–123.
[67] J. Kim, J.E. Lee, J. Lee, Y. Jang, S.W. Kim, K. An, J.H. Yu, T. Hyeon, Generalized fabrication of multifunctional nanoparticle assemblies on silica spheres, Angew Chem Int Ed Engl 45 (2006) 4789–4793.
[68] D. Bobo, K.J. Robinson, J. Islam, K.J. Thurecht, S.R. Corrie, Nanoparticle-based medicines: a review of FDA-approved materials and clinical trials to date, Pharm. Res. 33 (2016) 2373–2387.
[69] B. Fadeel, A.E. Garcia-Bennett, Better safe than sorry: understanding the toxicological properties of inorganic nanoparticles manufactured for biomedical applications, Adv. Drug Deliv. Rev. 3 (2009) 362–374.
[70] B. Tian, Q. Wang, Q. Su, W. Feng, F. Li, In vivo biodistribution and toxicity assessment of triplet-triplet annihilation-based upconversion nanocapsules, Biomaterials 112 (2017) 10–19.
[71] J. Yu, W. Yin, T. Peng, Y.N. Chang, Y. Zu, J. Li, X. He, X. Ma, Z. Gu, Y. Zhao, Biodistribution, excretion, and toxicity of polyethyleneimine modified NaYF4:Yb, Er upconversion nanoparticles in mice via different administration routes, Nanoscale 9 (2017) 4497–4507.
[72] C. Rome, J. Gravier, M. Morille, G. Divita, A.L. Bolcato-Bellemin, V. Josserand, J.L. Coll, Near-infrared optical imaging of nucleic acid nanocarriers in vivo, Methods Mol. Biol. 948 (2013) 49–65.
[73] K. Welsher, S.P. Sherlock, H. Dai, Deep-tissue anatomical imaging of mice using carbon nanotube fluorophores in the second near-infrared window, Proc. Natl. Acad. Sci. U. S. A. 108 (2011) 8943–8948.
[74] F. Ding, Y. Zhan, X. Lu, Y. Sun, Recent advances in near-infrared II fluorophores for multifunctional biomedical imaging, Chem. Sci. 9 (2018) 4370–4380.
[75] H. Wan, J. Yue, S. Zhu, T. Uno, X. Zhang, Q. Yang, K. Yu, G. Hong, J. Wang, L. Li, Z. Ma, H. Gao, Y. Zhong, J. Su, A.L. Antaris, Y. Xia, J. Luo, Y. Liang, H. Dai, A bright organic NIR-II nanofluorophore for three-dimensional imaging into biological tissues, Nat. Commun. 9 (2018) 1171.
[76] H.S. Choi, K. Nasr, S. Alyabyev, D. Feith, J.H. Lee, S.H. Kim, Y. Ashitate, H. Hyun, G. Patonay, L. Strekowski, M. Henary, J.V. Frangioni, Synthesis and in vivo fate of zwitterionic near-infrared fluorophores, Angew Chem Int Ed Engl 50 (2011) 6258–6263.
[77] B. Du, X. Jiang, A. Das, Q. Zhou, M. Yu, R. Jin, J. Zheng, Glomerular barrier behaves as an atomically precise bandpass filter in a sub-nanometre regime, Nat. Nanotechnol. 12 (2017) 1096–1102.
[78] Y. Huang, L. Fuksman, J. Zheng, Luminescence mechanisms of ultrasmall gold nanoparticles, Dalton Trans. 47 (2018) 6267–6273.
[79] H. Hyun, M.W. Bordo, K. Nasr, D. Feith, J.H. Lee, S.H. Kim, Y. Ashitate, L.A. Moffitt, M. Rosenberg, M. Henary, H.S. Choi, J.V. Frangioni, cGMP-compatible preparative scale synthesis of near-infrared fluorophores, Contrast Media Mol Imaging 7 (2012) 516–524.
[80] G. Lalwani, X. Cai, L. Nie, L.V. Wang, B. Sitharaman, Graphene-based contrast agents for photoacoustic and thermoacoustic tomography, Photo-Dermatology 1 (2013) 62–67.
[81] J. Weber, P.C. Beard, S.E. Bohndiek, Contrast agents for molecular photoacoustic imaging, Nat. Methods 13 (2016) 639–650.
[82] Y. Liu, J. He, K. Yang, C. Yi, Y. Liu, L. Nie, N.M. Khashab, X. Chen, Z. Nie, Folding up of gold nanoparticle strings into plasmonic vesicles for enhanced photoacoustic imaging, Angew. Chem. Int. Ed. 54 (2015) 15809–15812.
[83] G. Shim, S. Ko, D. Kim, Q.-V. Le, G.T. Park, J. Lee, T. Kwon, H.-G. Choi, Y.B. Kim, Y.-K. Oh, Light-switchable systems for remotely controlled drug delivery, J. Control. Release 267 (2017) 67–79.
[84] J.G. Fujimoto, C. Pitris, S.A. Boppart, M.E. Brezinski, Optical coherence tomography: an emerging technology for biomedical imaging and optical biopsy, Neoplasia (New York, N.Y.) 2 (2000) 9–25.
[85] M. Adhi, J.S. Duker, Optical coherence tomography – current and future applications, Curr. Opin. Ophthalmol. 24 (2013) 213–221.
[86] J.M. Tucker-Schwartz, K.R. Beavers, W.W. Sit, A.T. Shah, C.L. Duvall, M.C. Skala, In vivo imaging of nanoparticle delivery and tumor microvasculature with multimodal optical coherence tomography, Biomed Opt Express 5 (2014) 1731–1743.
[87] H. Hyun, M.H. Park, E.A. Owens, H. Wada, M. Henary, H.J. Handgraaf, A.L. Vahrmeijer, J.V. Frangioni, H.S. Choi, Structure-inherent targeting of near-infrared fluorophores for parathyroid and thyroid gland imaging, Nat. Med. 21 (2015) 192–197.
[88] F. Bolze, S. Jenni, A. Sour, V. Heitz, Molecular photosensitisers for two-photon photodynamic therapy, Chem Commun (Camb) 53 (2017) 12857–12877.
[89] H.J. Cho, M. Chung, M.S. Shim, Engineered photo-responsive materials for near-infrared-triggered drug delivery, J. Ind. Eng. Chem. 31 (2015) 15–25.
[90] H. Jin, M.G. Kim, S.B. Ko, D.H. Kim, B.J. Lee, R.B. Macgregor, Jr, G. Shim, Y.K. Oh, Stemmed DNA nanostructure for the selective delivery of therapeutics, Nanoscale 10 (2018) 7511–7518.
[91] P.K. Jain, I.H. El-Sayed, M.A. El-Sayed, Au nanoparticles target cancer, Nano Today 2 (2007) 18–29.
[92] X. Jing, Y. Mengxiao, P. Chuanqi, C. Phoebe, T. Jia, N. Xuhui, Z. Qinhan, T. Qiu, Z. Greg, D. Anthony, J. Xingya, K. Payal, H. Jer-Tsong, Z. Xudong, L. Pengyu, Z. Jie, Dose dependencies and biocompatibility of renal clearable gold nanoparticles: from mice to non-human primates, Angew. Chem. Int. Ed. 57 (2018) 266–271.
[93] J. Liu, P.N. Duchesne, M. Yu, X. Jiang, X. Ning, R.D. Vinluan 3rd, P. Zhang, J. Zheng, Luminescent gold nanoparticles with size-independent emission, Angew Chem Int Ed Engl 55 (2016) 8894–8898.
[94] J. Xu, M. Yu, C. Peng, P. Carter, J. Tian, X. Ning, Q. Zhou, Q. Tu, G. Zhang, A. Dao, X. Jiang, P. Kapur, J.T. Hsieh, X. Zhao, P. Liu, J. Zheng, Dose dependencies and biocompatibility of renal clearable gold nanoparticles: from mice to non-human primates, Angew Chem Int Ed Engl 57 (2018) 266–271.
[95] Y.X. Wang, Y. Choi, Z. Chen, S. Laurent, S.L. Gibbs, Molecular imaging: from bench to clinic, Biomed. Res. Int. 2014 (2014), 357258.
[96] J.J. Richardson, K. Liang, K. Kempe, H. Ejima, J. Cui, F. Caruso, Immersive polymer assembly on immobilized particles for automated capsule preparation, Adv. Mater. 25 (2013) 6874–6878.
[97] S.E. Gratton, P.D. Pohlhaus, J. Lee, J. Guo, M.J. Cho, J.M. Desimone, Nanofabricated particles for engineered drug therapies: a preliminary biodistribution study of PRINT nanoparticles, J. Control. Release 121 (2007) 10–18.